



UNIVERSITY OF LEEDS

This is a repository copy of *Characterization of the Gas-Bearing Tight Paleozoic Sandstone Reservoirs of the Risha Field, Jordan: Inferences on Reservoir Quality and Productivity*.

White Rose Research Online URL for this paper:

<https://eprints.whiterose.ac.uk/id/eprint/212029/>

Version: Accepted Version

Article:

Farouk, S., Qteishat, A., Sen, S. orcid.org/0000-0002-2796-4737 et al. (4 more authors) (2025) Characterization of the Gas-Bearing Tight Paleozoic Sandstone Reservoirs of the Risha Field, Jordan: Inferences on Reservoir Quality and Productivity. *Arabian Journal for Science and Engineering*, 50. pp. 215-235. ISSN 2193-567X

<https://doi.org/10.1007/s13369-024-09000-x>

© King Fahd University of Petroleum & Minerals 2024. This version of the article has been accepted for publication, after peer review (when applicable) and is subject to Springer Nature's AM terms of use (<https://www.springernature.com/gp/open-research/policies/accepted-manuscript-terms>), but is not the Version of Record and does not reflect post-acceptance improvements, or any corrections. The Version of Record is available online at: <http://dx.doi.org/10.1007/s13369-024-09000-x>.

Reuse

Items deposited in White Rose Research Online are protected by copyright, with all rights reserved unless indicated otherwise. They may be downloaded and/or printed for private study, or other acts as permitted by national copyright laws. The publisher or other rights holders may allow further reproduction and re-use of the full text version. This is indicated by the licence information on the White Rose Research Online record for the item.

Takedown

If you consider content in White Rose Research Online to be in breach of UK law, please notify us by emailing eprints@whiterose.ac.uk including the URL of the record and the reason for the withdrawal request.



eprints@whiterose.ac.uk
<https://eprints.whiterose.ac.uk/>

[Click here to view linked References](#)

1 **Characterization of the gas-bearing tight Paleozoic sandstone reservoirs of**
2 **the Risha field, Jordan – Inferences on reservoir quality and productivity**

3
4
5
6 4 Sherif Farouk^a, Abdelrahman Qteishat^b, Souvik Sen^{c*}, Fayez Ahmad^d, Khaled El-Kahtany^e,
7 Richard Collier^f, Mohammad A. Sarhan^g
8

9
10
11 7 ^a Exploration Department, Egyptian Petroleum Research Institute (EPRI), 1 Ahmed El-Zomor
12 Street, Nasr City, Cairo, Egypt
13

14
15 9 ^b Chemical Engineering Department, Al-Huson University College, Al- Balqa' Applied
16 University, Jordan
17

18
19
20 11 ^c Reservoir Technical Services (RTS), Baker Hughes, Mumbai, Maharashtra, India
21

22 12 ^d Prince El-Hassan Bin Talal Faculty of Natural Resources and Environment, Department of
23 Earth and Environmental Sciences, The Hashemite University, Zarqa, Jordan
24

25
26 14 ^e Geology and Geophysics Department, College of Science, King Saud University, Saudi
27 Arabia
28

29
30 16 ^f School of Earth and Environment, University of Leeds, Leeds LS2 9JT, UK
31

32 17 ^g Geology Department, Faculty of Science, Damietta University, 34517, Egypt
33

34
35 18
36 19 *Corresponding author: souvikseniitb@gmail.com
37

33 **Abstract**

34

35 This study presents the petrographical and petrophysical characteristics of the Cambro-
36 Ordovician clastic reservoirs from the Risha field, north-eastern Jordan. Routine core
37 analysis, wireline logs, petrographic thin sections, scanning electron microscopy, and X-ray
38 diffraction were integrated to characterize the gas reservoirs of the Risha, Dubeidib, and
39 Umm Sahn formations (the equivalent of Sarah, Qasim, and Upper Saq formations of
40 northern Saudi Arabia). These reservoirs are variably micro- and mesoporous, with
41 permeability < 1 mD and dominantly < 6% porosity. Wireline log-based assessment exhibits
42 low shale volume (< 30%), and high hydrocarbon saturation (45-95 %) in these tight
43 reservoirs. Petrographic investigation reveals that these reservoirs are fine-grained
44 sandstones, moderately sorted with high mineralogical maturity. The Risha and Dubeidib
45 reservoirs are subarkose while the Umm Sahn reservoir is composed of quartz arenite. The
46 late diagenetic silica cementation is inferred as reservoir quality-reducing diagenetic factor,
47 with quartz overgrowth of >10% corresponding to < 4% porosity. SEM images exhibit the
48 presence of grain-coating, pore-filling, and pore-lining chlorite and illite phases which hinder
49 quartz overgrowth and had a positive effect in retaining the primary porosity. The sandstones
50 with >20% clay-coating coverage corresponds to a lower quartz overgrowth (< 5%) and
51 therefore higher intergranular porosity (> 5%). Locally sutured grain contacts and stylolites
52 are observed which indicates intense chemical compaction. The feldspar grains are observed
53 to be partially dissolved, which generated minor secondary porosity. Micropore-dominated
54 pore systems and rare secondary macroporosity are typically isolated by abundant cement
55 and/or pore throats choked by clay minerals.

56

57 **Keywords:** Petrography; diagenesis; petrophysics; tight sand; Risha field; Paleozoic tight
58 reservoir.

59

60

61

62 **1 Introduction**

63

64 Tight gas sands account for more than two-thirds of global unconventional production [1].

65 These refer to low-permeability sandstones that produce dry natural gas [2]. The Middle East

66 and Africa host roughly 823 trillion cubic feet of tight sand gas reserves [1, 3]. The

67 Cambrian-Ordovician glacial sandstones of the Middle East and North Africa hold a large

68 tight sand gas potential. For example, the Paleozoic Hamra Quartzites are one of the most

69 prominent producing reservoir intervals in the Saharan basins of Algeria [4-6]. The Upper

70 Ordovician sandstones of the Sarah Formation are also confirmed as a gas reservoir in central

71 and north-western Saudi Arabia [7-8]. The present study focuses on the equivalent Paleozoic

72 tight sandstone gas reservoirs of the Risha field, located in the northeastern part of Jordan,

73 near the Iraq border. To maximize the potential of the Lower Paleozoic reservoirs that are

74 part of the petroleum system in Jordan [9], thorough understanding of the properties and

75 hence reservoir quality of targeted pay zones needs to be established.

76 The Risha field is the most significant gas field in Jordan, presently contributing ~5 % of

77 domestic natural gas consumption for electricity generation [10]. Production started in 1989,

78 with a total gas reserve of 180 billion cubic feet [11-12]. Since 2019, Jordan's national oil

79 company has boosted exploration activity in the eastern desert area to reduce hydrocarbon

80 imports and the promising gas reserves of the Risha field have become the primary focus.

81 Past field development activities increased Risha production from 8 million cubic feet per

82 day in 2017 to 30 million cubic feet in 2021 from about 30 producing wells. The recent and

83 ongoing activity, which started in 2022, has targeted the drilling of six new wells within the

84 Risha field near the Iraq border to increase the field's production capacity up to 50 million
85 cubic feet per day [13].

86

87 The Risha field hosts potential reservoirs in Lower Paleozoic intervals [9], including the
88 deposits of well-stacked thin sheets of outwash fan deposits, with sediments delivered via
89 sub-glacial tunnel valleys [14]. Previously published studies from the region have focused on
90 the sequence stratigraphy and depositional environments of Silurian and Ordovician intervals
91 [14-26] and the organic geochemistry, and source rock characteristics of Silurian and
92 Cretaceous shales [22, 29]. Reservoir pore characteristics, the impact of fractures, and
93 reservoir heterogeneity in Upper Ordovician Sarah Formation tight gas sandstones,
94 equivalent to the Risha Formation in Jordan, have been the focus of several studies in Saudi
95 Arabia [8, 30]. However, a comprehensive characterization of reservoir properties and
96 hydrocarbon potential of the Lower Paleozoic formations of Jordan has not yet appeared in
97 the published literature. This work integrates information from wireline logs, core-based
98 petrophysical measurements, petrographic thin sections, scanning electron microscopy
99 (SEM), X-ray diffraction (XRD), and drilling data to characterize the Risha, Dubeidib, and
100 Umm Sahm sandstones in the study region. The objectives of this study are to: i) infer
101 porosity, permeability, and pore types, ii) establish key petrophysical properties (effective
102 porosity, shale volume, and water saturation), iii) describe petrographic characteristics, iv)
103 characterize mineralogical distribution, and v) assess the diagenetic processes that have
104 affected the reservoir qualities.

105

106

107 **2 Geologic Setting**

108

109 The studied Risha tight gas field is located on the tectonically active/unstable shelf region of
110 the Arabian plate [31] (Fig. 1). The Tabuk Basin of Saudi Arabia marks its eastern boundary.
111 The studied Risha field is characterized by a low structural dip and hydrocarbon
112 accumulations are characterized by stratigraphic traps, i.e., lateral facies pinch-outs [32]. The
113 major fault systems express this, generally trending south-north or southeast-northeast. may
114 have played a role in the initial construction of the tectonics during the Late Precambrian age.
115 Following the Infracambrian extension linked with Pan-African East African-Antarctic
116 Orogeny [33-34], the Paleozoic remained tectonically inactive. Compressional tectonics took
117 place during the Late Carboniferous, which resulted in the uplift and erosion of the Upper
118 Paleozoic sediments during the Hercynian Orogeny [35] as well as the reactivation of key
119 structural trends.

Figure 1 to be inserted here

121 A general lithostratigraphic column is presented in Fig. 2. The basin hosts Cambrian-Eocene
122 sediments approximately 6km thick, directly above the Precambrian volcanic basement [28].
123 Cambro-Ordovician sedimentation (Ram Group) is dominated by terrestrial to shelfal marine
124 siliciclastics [16, 36], of which the Umm Sahm Formation is the uppermost unit. The
125 Cambrian Salb, Umm Ishrin, and Disi formations of the Ram Group are dominated by a long-
126 lived and extensive braid plain with clastics deposited by northward-flowing streams, except
127 for the mid-Cambrian Burj Formation marine carbonates which represent the first Paleozoic
128 marine transgression in the region [36]. The Upper Cambrian-Ordovician is composed of
129 marine and non-marine sandstone-shale sequences and hosts the primary gas reservoirs of the
130 Risha field [14, 37]. The Disi and Umm Sahm formations of the Upper Cambrian to
131 Ordovician Ram Group include fluvial, braided channel sandstones but are interbedded with
132 a variety of shallow marine and tidally influenced sediments [36].

Figure 2 to be inserted here

133

1
2
3 134 The Middle to Upper Ordovician Dubeidib Formation, equivalent to the Qasim Formation in
4
5 135 NW Saudi Arabia [14] comprises marine argillaceous to sandy, storm-dominated shoreface
6
7
8 136 deposits which show characteristic cleaning-up, coarsening-upwards cycles forming a
9
10 137 hierarchy of progradational sequences and parasequence [38]. These shallowing-up packages
11
12
13 138 are laterally extensive parallel to the northern Gondwana continental margin.

14
15
16 139 The Risha Formation, equivalent to the Ammar Formation in southern Jordan and the
17
18 140 Sarah/Zarq Formation in Saudi Arabia [14], represents significant erosional and depositional
19
20
21 141 events related to Hinantian (Upper Ordovician) glacio-eustatic fluctuations and associated
22
23 142 growth and decay of the Gondwanan ice sheet [14]. In southern Jordan and parts of NW
24
25
26 143 Saudi Arabia, incised valleys are interpreted as sub-glacial tunnel valleys [24] formed during
27
28 144 ice expansion and glacio-eustatic lowstand conditions. These valleys are in the order of
29
30
31 145 1000m wide and >100 m deep [14]. They are interpreted to have supplied sands to the north
32
33 146 where the resulting stacked sandstone sheets can be correlated over tens of kilometers and are
34
35 147 therefore interpreted as stacked glacial outwash fan deposits. In northern Jordan, the lower
36
37
38 148 part of the Risha Formation infill of each valley commonly shows a fining-up, dirtying-up
39
40 149 retrogradational trend indicating transgression associated with ice sheet retreat, but with the
41
42
43 150 overall retrogradational trend incorporating individually coarsening-up parasequences.
44
45 151 Maximum flooding occurs in the Risha II unit of the Hirst & Khatatneh [14] scheme. Above
46
47
48 152 this, there is typically a progradational parasequence set to the top of the Risha Formation,
49
50 153 interpreted as recording the progressive filling and oceanward regression of shallow marine
51
52
53 154 to fluvial facies along the remnant incised valleys. Erosion driven by a glacial rebound in the
54
55 155 hinterland, as the ice sheet retreated, possibly associated with the reactivation of NW-SE
56
57 156 trending faults, may have enhanced sediment supply during this progradational phase.
58
59
60
61
62
63
64
65

157 A significant transgression led to the deposition of Mudawwara Formation shale all over
158 Jordan, as a result of the end of Ordovician glacial activity and the melting of ice by the Early
159 Silurian [24-25]. The Silurian shales of the Mudawwara Formation are the primary source
160 rocks [28] of the region. Where the hot shales of the Mudawwara Formation are buried more
161 deeply, they represent mature shales from which dry gas has been generated [28].

162 The top of the Silurian Khisheh Formation marks a regional unconformity that separates the
163 Paleozoic clastics from Mesozoic dolomites [28]. This unconformity demonstrates how the
164 Upper Paleozoic was eroded in response to Hercynian uplift and hence is missing in the
165 studied area. The Triassic, Cretaceous, and Palaeogene intervals are dominated by carbonate
166 deposits linked to the sea level rise of the Tethys Ocean and the development of a major
167 carbonate platform over a large area [32, 39-40]. In addition to the Mudawwara Formation
168 shales, other organic-rich shales are present in the Late Ordovician and Late Cretaceous
169 intervals.

170

171 **3 Data and methods**

172

173 This study utilizes wireline logs, routine core analysis (RCAL), petrographic thin sections,
174 SEM, XRD, and drilling data to characterize the reservoir characteristics of the Risha,
175 Dubeidib, and Umm Sahn formations. RCAL provided porosity and horizontal permeability
176 measurements. Based on data availability, completeness, and formation coverage, four wells
177 were chosen for log-based quantitative petrophysical assessments, which are RH-3, RH-9,
178 RH-46, and RH-47. The wireline log suite includes gamma ray (GR), deep resistivity (Res),
179 bulk-density (RHOB), and neutron porosity (NPHI), which were utilized to estimate shale
180 volume (Vsh), effective porosity (PHIE) and water saturation (Sw). The latter was estimated
181 using gamma ray (GR) log data [41]:

182

1
2
3
4
5
6
7
8
9
10
11
12
13
14
15
16
17
18
19
20
21
22
23
24
25
26
27
28
29
30
31
32
33
34
35
36
37
38
39
40
41
42
43
44
45
46
47
48
49
50
51
52
53
54
55
56
57
58
59
60
61
62
63
64
65

$$V_{sh} = \frac{GR - GR_{min}}{GR_{max} - GR_{min}} \quad (1)$$

GR_{min} and GR_{max} are the minimum and maximum gamma ray values in a particular formation interval, respectively. PHIE was estimated based on V_{sh}, NPHI, and density-derived total porosity. Sw was inferred following the Indonesian model [42]:

$$S_w = \left\{ \frac{\sqrt{\frac{1}{R_{es}}}}{\left\{ \left(\frac{V_{sh}^{1-0.5} V_{sh}}{\sqrt{R_{sh}}} \right) + \sqrt{\frac{\Phi_e^m}{a R_w}} \right\}} \right\}^{\frac{2}{n}} \quad (3)$$

R_{sh} = shale resistivity, taken as 5 Ωm; R_w = resistivity of the connate water, taken as 0.03 Ωm; ‘a’ is tortuosity factor (considered a=1); ‘m’ and ‘n’ are cementation exponent and saturation exponents, respectively, with an assumed value of 2. Due to the tight nature of the sandstones, a porosity cut-off of 5% was considered to distinguish reservoir pay zones along with 30 % V_{sh} and 55 % S_w cut-offs. Lithology and hydrocarbon effects were analyzed from the RHOB-NPHI cross-plot. Spectral gamma-ray data was recorded in the well RH-47, which provided Thorium (Th) and Potassium (K) concentration. A cross-plot between ‘Th’ and ‘K’ was utilized to infer clay mineralogy.

A total of 20 thin sections were prepared from selected core samples and examined using an Olympus BX53P petrographic polarizing microscope. The thin sections were impregnated with blue dyed resin to facilitate the porosity identification. The staining methods by Dickson [55] were followed, using a mixed Alizarin Red-S and Potassium Ferri Cyanide solution to identify the carbonate minerals in the studied samples. Petrographic thin sections of the three reservoirs were available from the wells RH-23, RH-25, and RH-47. Out of 25 thin sections,

10 were available from the Risha Sandstone reservoirs, and 5 each from the Dubeidib and Umm Sahn reservoirs. Based on the modal point-count analysis of 200 counts per thin section, the constituting detrital components, cement and clay minerals, and pore types were inferred. Clay-coating coverage (in %) was estimated following the method proposed by Dutton et al. [58]. Scanning Electron Microscopy (SEM) analysis was carried out on a total of 10 samples using a Quanta FFG-450 SEM instrument in Jordanian Nanotechnology Institute. SEM photographs were available only for the Risha Formation in the well RH-29 which provided high-resolution information about the cement and clay mineralogy and their distribution. Based on the thin section and SEM evaluations, diagenetic factors were inferred together with their effects on reservoir quality. XRD data yielded further information on the whole rock composition and clay fraction. XRD analysis was performed on a total of 33 samples, that include 23 samples from the Risha Formation, 7 from the Dubeidib Formation and 3 from Umm Sahn Formation. A Bruker D8 advance diffractometer was utilized to conduct XRD analysis which provided the whole rock composition. This is a destructive analysis technique involving grinding a small rock sample (around 10 grams) to a fine powder for whole rock analysis. Drilling reports were available from the two wells RH-7 and RH-16, which were the best gas-producing wells in the Risha field. Drilling loss events (number of events, loss rate, and cumulative mud loss volume) were summarized the possible effects of fractures on reservoir productivity.

4 Results

4.1 Petrophysical analysis

231 The quantitative and qualitative petrophysical assessments of the Risha, Dubeidib, and Umm
232 Sahm formations were performed based on the core measurements and wireline log analysis.
233 An RCAL-based porosity against permeability cross-plot is presented for the three formations
234 in Fig. 3. The data are quite scattered, and a confident poro-perm relationship could not be
235 achieved; however, the majority of the data distribution indicates horizontal permeability of
236 less than 1 mD and porosity ranging between 1-10%, dominantly < 6% (Fig. 3). This is
237 indicative of the very tight nature of all the three Paleozoic intervals. Following the Winland
238 model-based pore throat radius (R35) estimates, we infer $0.1 \mu\text{m} \leq R3 \leq 2 \mu\text{m}$, which
239 satisfies the majority of the data distribution. This inferred R35 range indicates the
240 dominance of micro- and mesoporosities. Careful observation indicates that the Umm Sahm
241 Formation primarily demonstrates of mesoporosity (Fig. 3).

Figure 3 to be inserted here

244 Based on the wireline log data coverage, we analyzed the key petrophysical properties of the
245 Risha Formation from four wells, i.e., RH-3 (2610-2695 m, Fig. 4), RH-9 (2590-2670 m, Fig.
246 5), RH-46 (2560-2615 m, Fig. 6) and RH-47 (2580-2680 m, Fig. 7). The promising reservoir
247 intervals in the Dubeidib Formation are located between depths of 3442-3456 m in the RH-3
248 well (Fig. 8) and 3320-3341 m in the RH-47 well (Fig. 9). Potential Umm Sahm reservoir
249 sands were identified in RH-3 between 4025-4085 m (upper zone, Fig. 10) and 4115-4160 m
250 (lower zone, Fig. 11).

Figure 4 to be inserted here

Figure 5 to be inserted here

Figure 6 to be inserted here

255
1
2
3
4
5
6
7
8
9
10
11
12
13
14
15
16
17
18
19
20
21
22
23
24
25
26
27
28
29
30
31
32
33
34
35
36
37
38
39
40
41
42
43
44
45
46
47
48
49
50
51
52
53
54
55
56
57
58
59
60
61
62
63
64
65

Figure 7 to be inserted here

Figure 8 to be inserted here

Figure 9 to be inserted here

Figure 10 to be inserted here

Figure 11 to be inserted here

Based on the Gamma-ray cut-off of ~75 GAPI, the Risha reservoir zones in all four wells (RH-3, RH-9, RH-46, and RH-47) indicate two clean sand intervals separated by 10-20 m of shales, which demarcates a vertical flow barrier (Figs. 4-7). The interpreted hydrocarbon-bearing zones in the three formations are characterized by the small amount of shale volume, which is evidenced by the low gamma-ray ($GR < 75$ GAPI), along with high deep resistivity ($Res \sim 200 \Omega m$) and the cross-over between neutron porosity and bulk-density indicating presence of gas. The gas effect was also observed in the density-neutron cross-plots from all three studied formations (Figs. 12-14), where the majority of the data points are clustering around and above the sandstone line, indicating a sandy matrix. These reservoir zones exhibit 3-30% shale volume, 4-15% effective porosity (PHIE), 5-55% water saturation, and 45-95% gas saturation (Table 1).

Figure 12 to be inserted here

Figure 13 to be inserted here

Figure 14 to be inserted here

Table 1 to be inserted here

276 The potassium-thorium concentrations available from spectral gamma-ray data of the Risha
277 and Dubeidib intervals display mixed-layer clay and montmorillonite as the dominant clay
278 phases in the examined wells (Figs. 15-16).

279

280 **Figure 15 to be inserted here**

281 **Figure 16 to be inserted here**

282

283

284 **4.2 Petrographic investigation**

285

286 The Risha Sandstone is light-dark grey, very hard, brittle, and dominantly composed of very
287 fine-to-fine, sub-angular to sub-rounded, moderately sorted quartz grains along with
288 subordinate amounts of K-feldspar, trace amounts of mica and heavy minerals (Fig. 17a-d).

289 The silica cementation is commonly observed in all the Risha Sandstone (up to 12% in the
290 Risha Sandstone and up to 18 % in the Umm Sahn Sandstone, based on the point count data)
291 that filled the pore spaces (Figs. 17b-c). Pore-filling carbonate cement (i.e., dolomite, Fig.
292 17b-c), diagenetic clay filling (Fig. 17d), and chlorite rims surrounding the quartz grains
293 (Figs. 17b-d) are commonly observed in all the thin sections. The framework grains are
294 tightly packed with very minor interparticle macroporosity. The feldspar grains are observed
295 to be partially altered and dissolved (Figs. 17c-d).

296

297 **Figure 17 to be inserted here**

298

299 The SEM images of the Risha Sandstone exhibit the presence of chlorite and illite clay
1
2 300 phases which mostly occur as grain-coating, pore-filling, and pore-lining forms (Figs. 18a-c).
3
4 301 Chlorite fills are coarser in the central part of the pores than the peripheries (Fig. 18a).
5
6
7 302 Carbonate (Figs. 18d) and quartz (Fig. 18b) cementation are also observed in SEM.
8
9
10 303 Carbonate cements exhibit developed cleavage planes (Figs. 18d).
11

12 304
13
14 **Figure 18 to be inserted here**
15

16
17 306
18
19
20 307 The Dubeidib reservoirs are composed of mostly argillaceous sandstones with siltstones and
21
22 308 clay interbeds. In thin sections the argillaceous sandstone exhibits a starry night appearance
23
24
25 309 characterized by very fine-grained quartz and laminated clay fabrics (Fig. 19a). Quartz is the
26
27 310 dominant framework grain, followed by plagioclase and K-feldspars. Partially altered
28
29
30 311 feldspars and pore-filling clay are observed along with minor dolomites (Fig. 19b). Grain-
31
32 312 coating chlorite rims are observed. Primary interparticle porosity and minor intraparticle
33
34
35 313 porosity created by feldspar dissolution are observed in the Dubeidib Sandstone samples.
36

37 314
38
39
40 **Figure 19 to be inserted here**
41

42
43 316
44
45
46 317 The Umm Sahn Sandstone is primarily composed of fine-to-medium-grained, moderately
47
48 318 well-sorted quartz with traces of heavy minerals (Fig. 20a-b). Locally sutured grain contacts
49
50
51 319 and stylolites are observed (Fig. 20a). Umm Sahn Sandstone exhibits extensive quartz
52
53 320 cementation in all samples (up to 18 % based on point count data). The chlorite rims around
54
55
56 321 quartz grains and minor pore-filling detrital clay materials are also observed, comparatively
57
58 322 lesser than the Risha and Dubeidib samples. Micropore-dominated pore systems and rare
59
60
61
62
63
64
65

323 secondary macroporosity are typically isolated by abundant cement and/or choked by clay
1
2 324 minerals.

3
4
5 325

6
7
8 326 **Figure 20 to be inserted here**

9
10
11 327

12
13 328 The QFR plot is presented in Fig. 21, based on the sandstone classification system by Folk
14
15 329 [57]. Compositionally the Risha and Dubeidib sandstones are arkose and Umm Sahn
16
17 330 Sandstone is quartz arenite (Fig. 21). The XRD results are presented in Fig. 22, which specify
18
19 331 that quartz is the dominant mineral phase in all three formations, followed by feldspar with
20
21 332 minor carbonate and siderite. The quartz percentage is highest in the Umm Sahn Sandstone
22
23 333 (Fig. 22a), while the Dubeidib Sandstone contains a higher concentration of feldspar when
24
25 334 compared with the other two formations (Fig. 22b). The Umm Sahn interval is almost devoid
26
27 335 of feldspars and carbonates. The clay content is highest in the Dubeidib Formation and lowest
28
29 336 in the Umm Sahn Formation, as was also observed in the thin sections. Chlorite and illite are
30
31 337 the dominant clay phases, as identified in XRD as well as SEM.
32
33
34
35
36
37

38 338

39
40 339 **Figure 21 to be inserted here**

41
42
43 340 **Figure 22 to be inserted here**

44
45
46 341

47 342 **5 Discussion**

48 49 343 **5.1 Diagenesis of the Paleozoic reservoirs**

50
51
52 344

53
54
55
56 345 All the three studied reservoir intervals exhibit very strong diagenetic imprints which
57
58 346 significantly influenced the intergranular porosity of the studied sandstones. Compaction,
59
60
61

1 347 cementation, and feldspar dissolution are identified as the three diagenetic processes affecting
2
3 348 the Paleozoic reservoir quality in the Risha tight gas field. The paragenetic sequence is
4
5 349 presented in Fig. 23. Following deposition, the sandstones were compacted, that resulted in
6
7 350 tighter grain packing. Mechanical compaction continued throughout the burial. Mechanical
8
9 351 compaction is evident based on the concavo-convex and long straight grain contacts (Fig.
10
11 352 17b, d) as well as the overall tight packing of quartz grains. During the early diagenetic
12
13 353 phase, grain-coating chlorite rims were developed. Clay cementation is commonly observed
14
15 354 in all the thin sections. Chlorite and illite are the dominant clay phases which can have
16
17 355 authigenic or detrital origin. These clay minerals occur as pore-lining and pore-filling forms,
18
19 356 as seen from thin sections as well as SEM images (Figs. 17d, 18a-c, 19b, and 20a-b). Chlorite
20
21 357 mostly occurs as grain coatings surrounding the quartz framework grains in all three
22
23 358 reservoirs, which are usually formed in the early diagenesis period [43, 49]. Such clay forms
24
25 359 are extensively reported from clastic reservoirs globally [49-51].
26
27
28
29
30

31
32
33
34 361 **Figure 23 to be inserted here**
35
36

37 362
38
39 363 Feldspar dissolution was observed in the thin section, which might have taken place during
40
41 364 and immediately after the initial diagenetic phase. The occurrence of fresh as well as partially
42
43 365 dissolved feldspar within the same reservoir may indicate pre-depositional weathering at the
44
45 366 sediment source or post-depositional selective alteration [19-20, 32]. Partial dissolution of
46
47 367 feldspar contributes to secondary porosity generation and may be considered a reservoir
48
49 368 quality-enhancing diagenetic agent [56, 59-60]. This effect was limited to the Risha and
50
51 369 Dubeidib intervals, while the Umm Sahn Sandstone is almost devoid of feldspar (as seen
52
53 370 from XRD, Figs. 21a-b). Cementation is observed as the dominant diagenetic factor. Thin
54
55 371 sections and SEM images indicate extensive silica cementation and minor carbonate
56
57
58
59
60
61
62
63
64
65

372 cementation in the pore spaces which significantly decreased the porosity and hence reservoir
373 quality. Carbonate cement precipitation may occur in a shallow marine setting or during
374 burial. The dolomites observed in the thin sections might have been formed from the
375 precursor carbonate material by dolomitization facilitated by moderate burial. At the late
376 diagenetic stage, silica cementation might have occurred in deep burial conditions. This is
377 generally facilitated by higher temperature conditions [45], but quartz dissolution and
378 consequent availability for reprecipitation also increase rapidly with temperatures above ~
379 100°C [46-48]. The Umm Sahn Sandstone exhibits long sutured grain contacts and stylolites
380 indicating intense chemical compaction (Fig. 20a), and therefore pressure solution at the
381 quartz grain contacts is possibly the major source of silica cement at the later stages of the
382 diagenesis.

383

384 **5.2 Effects of diagenesis on reservoir quality**

385 The two main diagenetic factors that influenced the studied reservoirs are clay cementation at
386 the early diagenetic phase and silica cementation in the late diagenetic stage. The silica
387 cementation negatively affects the reservoir porosity. However, the clay coatings can raise
388 the reservoir's compressive strength [52] and hinder quartz overgrowths, and potentially
389 reduce further porosity loss [53-54, 59-60]. To understand this effect, please refer to Figs. 24-
390 25 that present the cross plots using point count data in relation to the intergranular porosity.
391 The cross-plot between clay-coating coverage (%) and intergranular porosity indicates a
392 positive correlation where the samples with > 80 % clay-coating coverage indicates the
393 intergranular porosity of more than 5 % (Fig. 24a), while the samples with higher clay-
394 coating coverage exhibit strongly negative correlation with the quartz overgrowth by silica
395 cementation (Fig. 25b). The Dubeidib Sandstone shows a higher clay-coating coverage of >
396 75% and these have a lower quartz overgrowth (< 5%), while the Umm Sahn Sandstone

397 exhibits the highest quartz overgrowth (up to 18 %), associated with lesser clay-coating
398 coverage (< 75 %) (Fig. 25b). Based on the point count data, the Dubeidib Sandstone samples
399 exhibit the higher amount of total pore-filling clay up to 18%. Based on the 15 thin sections,
400 we do not see a very strong correlation between total volume of pore-filling clay and
401 intergranular porosity. However, due to the pore-filling habit, the clay minerals generally
402 have a negative impact on the reservoir quality. The late diagenetic silica cementation shows
403 a strongly negative correlation with reservoir porosity. The Risha and Umm Sahn
404 Sandstones with quartz overgrowth of > 10% show intergranular porosity below 4% (Fig.
405 25a).

407 **Figure 24 to be inserted here**

408 **Figure 25 to be inserted here**

410 **5.3 Petrophysical quality and reservoir productivity – inferences for reservoir** 411 **development**

413 The wireline log-based quantitative assessments indicate good reservoir petrophysical
414 qualities in terms of shale volume and water saturation. The Paleozoic reservoirs are
415 characterized by their clean nature (low shale volume, below 0.3 dec) and high hydrocarbon
416 saturation ranging between 0.45-0.95dec and dominantly above 0.75 dec. Gas effects are
417 commonly observed in the petrophysical cross-plots (Figs. 12-14). However, routine core
418 analysis has determined very poor porosity (mostly < 5%) and tight permeability below 1
419 mD, dominated by micro- and mesoporosities (Fig. 3). Poor effective porosity was also
420 observed from wireline log-based estimates, which is usually between 0.06-0.12 dec.
421 Extensive silica cementation is the dominant diagenesis mechanism behind the tight nature of

1
2 422 these gas-bearing sandstones. Feldspar dissolution did not have much positive effect on
3 423 porosity enhancement.

4
5 424
6
7 425 We observed very thin high-angle fractures within the cores (Fig. 26a-c) of the Risha and
8
9 426 Umm Sahm intervals. Open natural fractures generally provide efficient flow pathways in
10
11 427 such tight reservoirs, however, the thin sub-vertical fractures seen on the cores are calcite-
12
13 428 filled, and these calcite-filled fractures will not contribute much to the reservoir permeability.
14
15
16 429 However, an open fracture network can be present locally which could significantly improve
17
18
19 430 reservoir permeability.

20
21
22 431
23
24 432 **Figure 26 to be inserted here**

25
26
27 433
28
29
30 434 To understand the presence and role of fractures, we investigated the drilling history of some
31
32 435 of the best-producing wells in the Risha gas field, i.e., RH-7 and RH-16. Partial mud loss
33
34 436 events were reported from these two wells while drilling the Paleozoic Risha reservoir
35
36
37 437 section. RH-7 experienced 40 loss events with a cumulative mud loss volume of around
38
39 438 14000 barrels, while ~4500 barrel mud loss was reported from 14 events in the well RH-16
40
41
42 439 (Fig. 27). These observations indicate the possible presence of fractured intervals which
43
44 440 contributed to the mud losses during drilling. The high productivity of these two wells (RH-7
45
46
47 441 and RH-6) confirms the presence of excellent permeability zones within the Risha interval.

48
49 442
50
51 443 **Figure 27 to be inserted here**

52
53
54 444
55
56
57 445 Due to the unavailability of the wireline logs, the lithological interpretation of these two wells
58
59 446 could not be presented. But the drilling report and mudlog indicates dominantly sandstone

447 intervals with minor shale intercalation, which is a typical characteristic of the Risha
448 Formation, as can be seen from the presented petrophysical logs of RH-3 (Fig. 4), RH-9 (Fig.
449 5), RH-46 (Fig. 6) and RH-57 (Fig. 7). The first loss events were encountered in the wells
450 RH-7 and RH-46 at around 2600m and 2650m, respectively (Fig. 23). The occurrence of first
451 loss events confirms the presence of fractured intervals at those depths (2600m in RH-7 and
452 ~2650m in RH-47). As losses continued while drilling the deeper section, it is difficult to
453 confirm from the loss data if further fractured intervals are present below the first loss zone.
454 Based on the drilling experienced, two subsurface scenarios are possible therefore: i)
455 fractures are only present in the zone where the first loss was reported, and that same interval
456 consistently experienced mud loss while drilling further, and ii) along with the first fractured
457 interval (interval with first reported losses), there are multiple similar zones with fracture-
458 enhanced permeability, which repeatedly exhibited multiple loss events. It is to be noted that
459 the drilling data (loss depths and loss volumes) cannot alone confirm and identify all the
460 potentially fractured zones. Image logs and production logging data are more suitable inputs
461 to confirm the same. Mapping the fractured intervals and characterization of the fracture
462 geometry is critical, especially while dealing with such tight sandstone reservoirs. We highly
463 recommend running wireline image logging tools in the upcoming wells which would be able
464 to capture such fractures.

6 Conclusions

1
2
3
4
5
6
7
8
9
10
11
12
13
14
15
16
17
18
19
20
21
22
23
24
25
26
27
28
29
30
31
32
33
34
35
36
37
38
39
40
41
42
43
44
45
46
47
48
49
50
51
52
53
54
55
56
57
58
59
60
61
62
63
64
65

471 This study characterizes the reservoir properties of the gas-bearing Cambro-Ordovician
472 sandstones from the Risha field, Jordan. The quartz-arenites and subarkosic reservoirs of the
473 Risha, Dubeidib, and Umm Sahn formations exhibit high mineralogical maturity and
474 moderate textural maturity. All the reservoirs are extensively affected by various diagenetic
475 factors including cementation (dominantly silica, minor carbonate, and clay) and compaction
476 (both mechanical and chemical) which reduce the reservoir storage and flow capacities.
477 Petrophysically these are very tight with < 6% porosity and have very poor horizontal
478 permeability (mostly < 1 mD). However, low shale volume and excellent hydrocarbon
479 saturation make these tight sandstones very good unconventional gas reservoirs, if necessary,
480 completion techniques are applied. Drilling events in a few high-performance wells (in terms
481 of production) indicate high-volume mud loss events, that might be caused by natural
482 fractures. We highly recommend acquiring image log data in the upcoming wells which will
483 provide a direct information about the geometries and effectiveness of any pre-existing
484 fracture sets. The studied cores only show some thin sub-vertical fractures filled with calcite
485 and these did not enhance the reservoir flow capacity. We envisage the possibility of
486 permeability improvement within the studied tight Paleozoic reservoirs under the influence of
487 natural or hydraulically created fractures. Necessary reservoir development strategies are
488 discussed based on petrophysical, and petrographical observations.

492 **Acknowledgments**

493
494 The authors are grateful to Dr. Bassam El Ali (managing editor) for the excellent editorial
495 handling. Three anonymous reviewers are thanked for their constructive review comments

496 which benefited the manuscript. The authors are grateful to the Al- Balqa' Applied
497 University, Jordan, and National Petroleum Company, Jordan for the facilities and data
498 provided for this work. This research was supported by King Saud University, Riyadh, Saudi
499 Arabia, Supporting Project number-RSP2024R139.

501 **References**

- 502
503 1. Khlaifat, A., Qutob, H., Barakat, N., 2010. Increasing the world's gas reserves by the
504 exploitation of unconventional tight gas reservoirs. In: SPE/PAPG Annual Technical
505 Conference, Islamabad, Pakistan, Nov 10-11. SPE-42842.
- 506 2. Holditch, S., 2006. Tight gas sands. *Journal of Petroleum Technology*, 58(6), 86-93.
507 SPE-103356-JPT.
- 508 3. Kawata, Y., Fujita, K., 2001. Some predictions of possible unconventional
509 hydrocarbons availability until 2100. In: SPE Asia Pacific Oil and Gas Conference
510 and Exhibition, Jakarta, Indonesia, Apr 17-19. SPE-68755.
- 511 4. Baouche, R., Ganguli, S.S., Sen, S., Radwan, A.E., 2023. Assessment of reservoir
512 stress state and its implications for Paleozoic tight oil reservoir development in the
513 Oued Mya Basin, northeastern Algerian Sahara. *Geosystems and Geoenvironment*,
514 2(1), 100112.
- 515 5. Baouche, R., Sen, S., Feriel, H.A., Radwan, A.E., 2022. Estimation of horizontal
516 stresses from wellbore failures in strike-slip tectonic regime: A case study from the
517 Ordovician reservoir of the Tinzaouatine Field, Illizi Basin, Algeria. *Interpretation*,
518 10(3), SF37-SF44.
- 519 6. Baouche, R., Sen, S., Chaouchi, R., Ganguli, S.S., 2021. Modeling in-situ tectonic
520 stress state and maximum horizontal stress azimuth in the Central Algerian Sahara –
521 A geomechanical study from EL Agreb, EL Gassi and Hassi Messaoud fields. *Journal*
522 *of Natural Gas Science and Engineering*, 88, 103831.
- 523 7. Bu-Khamseen, R., Khakimov, A., Sierra, L., Young, D. Machala, M., 2010. First
524 successful tight gas reservoir completion and fracture stimulation in Sarah Formation,
525 Rub Al-Khali Empty Quarter of Saudi Arabia. SPE Deep Gas Conference and
526 Exhibition, Manama, Bahrain, January 2010, SPE-130722.
527 <https://doi.org/10.2118/130722-MS>
- 528 8. Adebayo, A.R., Babalola, L., Hussaini, S.R., Alqubalee, A., Babu, R.S., 2019. Insight
529 into the Pore Characteristics of a Saudi Arabian Tight Gas Sand Reservoir. *Energies*,
530 12, 4302.
- 531 9. Naylor, D., Al-Rawi, M., Clayton, G., Fitzpatrick, M.J., Green, P.F., 2013.
532 Hydrocarbon potential in Jordan. *Journal of Petroleum Geology* 36, 205-236.

- 1 539 10. Journal of Petroleum Technology (JPT), 2021. Jordan Finds “Promising” Gas
2 540 Reserves Near Iraq Border. Report dated Feb 1, 2021.
3 541
- 4 542 11. Sorkhabi, R., 2009. Paleozoic tight gas plays in Jordan. GEO Expro.
5 543 <https://www.geoexpro.com/articles/2010/01/paleozoic-tight-gas-plays-in-jordan>
6 544
- 7 545 12. Luning, S., Kuss, J., 2014. Petroleum Geology of Jordan, in: Marlow, L., Kendall,
8 546 C.C.G., Rose, L.A. (Eds.), Memoir 106, Petroleum Systems of the Tethyan Region.
9 547 AAPG Special volume, 217-239.
10 548
- 11 549 13. Jordan Times (JT), 2021. Kharabsheh announces effort to drill 6 gas wells near Iraqi
12 550 border. Report, dated Dec 4, 2021.
13 551
- 14 552 14. Hirst, J.P.P. and Khatatneh, M., 2019. Depositional model for the distal Ordovician
15 553 glaciaded margin of Jordan; implications for the reservoir potential of the Risha
16 554 Formation. Geological Society, London, Special Publications, 475(1), 109-129.
17 555
- 18 556 15. Abed, A.M., Makhlof, I.M., Amireh, B.S., Khalil, B., 1993. Upper Ordovician
19 557 glacial deposits in southern Jordan. Episodes, 16, 316-328.
20 558
- 21 559 16. Amireh, B.S., Schneider, W., Abed, A.M., 2001. Fluvial-shallow marine-glaciofluvial
22 560 depositional environments of the Ordovician System in Jordan. Journal of Asian Earth
23 561 Sciences 19, 45-60.
24 562
- 25 563 17. Amireh, B.S., Schneider, W., Abed, A.M., 1994. Evolving fluvial-transitional-marine
26 564 deposition through the Cambrian sequence of Jordan. Sedimentary Geology, 89, 65-
27 565 90.
28 566
- 29 567 18. Makhlof, I., 1995. Tempestite facies displaying hummocky cross-stratification and
30 568 subaqueous channels in Ordovician shelf deposition, South Jordan. Journal of African
31 569 Geoscience Review, 2, 91-100.
32 570
- 33 571 19. Armstrong, H.A., Abbott, G.D., Turner, B.R., Makhlof, I.M., Muhammad, A.B.,
34 572 Pedentchouk, N. and Peters, H., 2009. Black shale deposition in an Upper
35 573 Ordovician– Silurian permanently stratified, peri-glacial basin, southern Jordan.
36 574 Palaeogeography, Palaeoclimatology, Palaeoecology, 273(3-4), pp.368-377.
37 575
- 38 576 20. Armstrong, H.A., Turner, B.R., Makhlof, I.M., Williams, M. and Abdulfattah Abu
39 577 Salah, A.A.S., 2005. Sequence stratigraphy and depositional environment of an Upper
40 578 Ordovician (Hirnantian), peri-glacial petroleum source rock. Palaeogeography,
41 579 Palaeoclimatology, Palaeoecology, 220, 273-289.
42 580
- 43 581 21. Luning, S., Shahin, Y.M., Loydell, D., Al-Rabi, H.T., Masri, A., Tarawneh, B. and
44 582 Kolonic, S., 2005. Anatomy of a world-class source rock: Distribution and
45 583 depositional model of Silurian organic-rich shales in Jordan and implications for
46 584 hydrocarbon potential. AAPG Bulletin, 89(10), 1397-1427.
47 585

- 584 22. Lüning, S., Craig, J., Loydell, D.K., Štorch, P. and Fitches, B., 2000. Lower Silurian
1 585 hot shales in North Africa and Arabia: regional distribution and depositional model.
2 586 Earth-Science Reviews, 49(1-4), 121-200.
3 587
- 588 23. Turner, B.R., Makhlof, I.M., Armstrong, H.A., 2005. Late Ordovician (Ashgillian)
6 589 glacial deposits in southern Jordan. *Sedimentary Geology* 181, 73-91.
7 590
8 591
- 592 24. Douilet, G., Ghienne, J.-F., Geraud, Y., Abueladas, A., Diraison, M., Al-Zoubi, A.
10 592 2012. Late Ordovician tunnel valleys in southern Jordan. In: Husse, M., Redfern, J.,
11 593 Le Heron, D.P., Dixon, R.J., Moscariello, A., Craig, J. (eds) *Glaciogenic Reservoirs*
12 594 *and Hydrocarbon Systems*. Geological Society, London, Special Publications, 368,
13 595 275-292.
14 596
15 596
- 597 25. Ghienne, J.-F., Desrochers, A. et al. 2014. A Cenozoic style scenario for the end-
17 598 Ordovician glaciation. *Nature Communications*, 5, 4485.
18 599
19 599
- 600 26. Farouk, S., Faris, M., Ahmad, F., Powell, J., 2015. New microplanktonic
21 601 biostratigraphy and depositional sequences across the Middle–Late Eocene and
22 602 Oligocene boundaries in eastern Jordan, *Geology*, 20 (3), 145-172.
23 603
24 603
- 604 27. Loydell, D.K., Butcher, A., Frýda, J., Lüning, S., Fowler, M., 2009. Lower Silurian
26 605 “hot shales” in Jordan: a new depositional model. *Journal of Petroleum Geology*,
27 606 32(3), 261-270.
28 607
29 607
- 608 28. Farouk, S., Lofty, N.M., Qteishat, A., Ahmad, F., Shehata, A.M., Al-Kahtany, K. and
31 609 Hsu, C.S., 2023. Source and thermal maturity assessment of the Paleozoic-Mesozoic
32 610 organic matter in the Risha gas field, Jordan. *Fuel*, 335, 126998.
33 611
34 611
- 612 29. Hakimi, M.H., Alqudah, M., Mustapha, K.A. Varfolomeev, M.A., Lashin, A., Hatem,
36 613 B.A., Rahim, A., Sen, S., Radwan, A.E., Yelwa, N.A., 2023. Early-Oil Generation
37 614 Potential of Type II-S Kerogen in the Upper Cretaceous (Cenomanian–Turonian)
38 615 Organic-Rich Carbonate Succession from Ajloun Region in Northern Jordan. *Arabian*
39 616 *Journal for Science and Engineering*, 48, 695-720.
40 617
41 617
42 617
- 618 30. El-Deek, I., Abdullatif, O., Korvin, G., 2017. Heterogeneity analysis of reservoir
44 619 porosity and permeability in the Late Ordovician glacio-fluvial Sarah Formation
45 620 paleovalleys, central Saudi Arabia. *Arabian Journal of Geosciences*, 10, 400.
46 621
47 621
- 622 31. Lotfy, N.M., Qteishat, A., Farouk, S., Ahmed, F., Al-Kahtany, K., Hsu, C.S., 2022.
49 623 Geochemical characteristics and genetic types of Ordovician tight gas in the Risha
50 624 Gas Field, Eastern Jordan based on carbon and hydrogen isotope compositions.
51 625 *Marine and Petroleum Geology*, 143, 105810.
52 626
53 626
- 627 32. Tamar-Agha, M.Y., 2009. The influence of cementation on the reservoir quality of the
55 628 Risha Sandstone Member (Upper Ordovician), Risha Gasfield, NE Jordan. *Journal of*
56 629 *Petroleum Geology*, 32(2), 193-208.
57 629
58
59
60
61
62
63
64
65

- 630 33. Jacobs, J., Thomas, R.J., 2004. Himalayan-type indenter-escape tectonics model for
1 631 the southern part of the late Neoproterozoic-early Paleozoic East African-Antarctic
2 632 region. *Geology*, 32(8), 721-724.
3
- 4 633 34. Kusky, T.M., Matsah, M.I., 2003. Neoproterozoic dextral faulting in the Najd Fault
5 634 System, Saudi Arabia, preceded sinistral faulting and escape tectonics related to
6 635 closure of the Mozambique Ocean. Geological Society, London, Special Publications,
7 636 206, 327-361.
8 637
- 9 638 35. Laboun, A.A., 2010. Paleozoic tectono-stratigraphic framework of the Arabian
10 639 Peninsula. *Journal of King Saud University (Science)*, 22, 41-50.
11 640
- 12 641 36. Powell, J.H., Abed, A.M., Le Nindre, Y.-M., 2014. Cambrian stratigraphy of Jordan.
13 642 *GeoArabia*, 19(3), 81-134.
14 643
- 15 644 37. Beydoun, Z.R., Futyan, A.R.I., Jawzi, A.H., 1994. Jordan revisited: Hydrocarbon
16 645 habitat and potential. *Journal of Petroleum Geology*, 17, 177-194.
17 646
- 18 647 38. Senalp, M.A. & Al-Duaiji, A.A., 2001. Qasim Formation: Ordovician Storm- and
19 648 Tide-Dominated Shallow-Marine Siliciclastic Sequences, Central Saudi Arabia.
20 649 *GeoArabia*. DOI: 10.2113/geoarabia0602233
21 650
- 22 651 39. Sadooni, F.N., Dalqamouni, A., 1998. Geology and petroleum prospects of Upper
23 652 Triassic sediments, Jordan. *Marine and Petroleum Geology*, 15, 783-801.
24 653
- 25 654 40. Lüning, S., Loydell, D.K., Storch, P., Shahin, Y., Craig, J., 2006. Origin, sequence
26 655 stratigraphy and depositional environment of an Upper Ordovician (Hirnantian)
27 656 deglacial black shale, Jordan - Discussion. *Palaeogeography, Palaeoclimatology,*
28 657 *Palaeoecology*, 230, 352-355.
29 658
- 30 659 41. Asquith, G., and Gibson, C., 1982. Basic well log analysis for geologists: methods in
31 660 Exploration series. AAPG, Tulsa, Oklahoma.
32 661
- 33 662 42. Poupon, A., and Leveaux, J., 1971. Evaluation of water saturation in shaly formations.
34 663 In SPWLA 12th annual logging symposium. Society of Petrophysicists and Well-Log
35 664 Analysts.
36 665
- 37 666 43. Lundegard, P.D., 1992. Sandstone porosity loss; a "big picture" view of the
38 667 importance of compaction. *J. Sediment. Res.* 62(2), 250-260.
39 668
- 40 669 44. Makeen, Y.M., Shan, X., Ayinla, H.A., Adepehin, E.J., Ayuk, N.E., Yelwa, N.A., Yi,
41 670 J., Elhassan, O.M.A., Fan, D., 2021. Sedimentology, petrography, and reservoir
42 671 quality of the Zarga and Ghazal formations in the Keyi oilfield, Muglad Basin, Sudan.
43 672 *Scientific Reports*, 11(1), 743.
44 673
- 45 674 45. Lai, J., Wang, G., Chai, Y., Xin, Y., Wu, Q., Zhang, X., Sun, Y., 2017. Deep burial
46 675 diagenesis and reservoir quality evolution of high-temperature, high-pressure
47 676 sandstones: examples from Lower Cretaceous Bashijiqike Formation in Keshen area,
48 677 Kuqa depression, Tarim basin of China. *AAPG Bulletin*, 101(6), 829-862.
49
50
51
52
53
54
55
56
57
58
59
60
61
62
63
64
65

678

- 1 679 46. Rimstidt, J.D., 1997. Quartz solubility at low temperatures. *Geochimica et*
2 680 *Cosmochimica Acta*, 61(13), 2553-2558.
- 3 681
- 4 682 47. Worden, R.H., Morad, S., 2000. Quartz cementation in oil field sandstones: a review
5 683 of the key controversies. In: Worden, R.H. and Morad, S. (Eds.), *Quartz Cementation*
6 684 *in Sandstones*. pp. 1-20. IAS Spec. Publ., 29. Blackwell Science, Oxford.
- 7 685
- 8 686 48. Bjørlykke, K., 1994. Pore water flow and mass transfer of solids in solution in
9 687 sedimentary basins. In: (Eds) Parker, A. and Sellwood, B.W., *Quantitative*
10 688 *Diagenesis: Recent Developments and Applications to Reservoir Geology*, 189-221,
11 689 Kluwer Dordrecht.
- 12 690
- 13 691 49. Freiburg, J.T., Ritzi, R.W., Kehoe, K.S., 2016. Depositional and diagenetic controls
14 692 on anomalously high porosity within a deeply buried CO₂ storage reservoir - the
15 693 Cambrian Mt. Simon sandstone, Illinois basin, USA. *Int. J. Greenh. Gas Control* 55,
16 694 42-54.
- 17 695
- 18 696 50. Dowey, P.J., Hodgson, D.M., Worden, R.H., 2012. Pre-requisites, processes, and
19 697 prediction of chlorite grain coatings in petroleum reservoirs: a review of subsurface
20 698 examples. *Marine and Petroleum Geology*, 32, 63-75.
- 21 699
- 22 700 51. Zhu, S., Wang, X., Qin, Y., Jia, Y., Zhu, X., Zhang, J., Hu, Y., 2017. Occurrence and
23 701 origin of pore-lining chlorite and its effectiveness on preserving porosity in sandstone
24 702 of the Middle Yanchang Formation in the Southwest Ordos basin. *Appl. Clay Sci.*
25 703 148, 25-38.
- 26 704
- 27 705 52. Spinelli, G.A., Mozley, P.S., Tobin, H.J., Underwood, M.B., Hoffman, N.W., Bellew,
28 706 G.M., 2007. Diagenesis, sediment strength, and pore collapse in sediment
29 707 approaching the Nankai Trough subduction zone. *GSA Bulletin*, 119 (3-4), 377-390.
- 30 708
- 31 709 53. Nguyen, B.T.T., Jones, S.J., Goult, N.R., Middleton, A.J., Grant, N., Ferguson, A.,
32 710 Bowen, L., 2013. The role of fluid pressure and diagenetic cements for porosity
33 711 preservation in Triassic fluvial reservoirs of the Central Graben, North Sea. *AAPG*
34 712 *Bulletin*, 97 (8), 1273-1302.
- 35 713
- 36 714 54. Cui, Y., Wang, G., Jones, S.J., Zhou, Z., Ran, Y., Lai, J., Li, R., Deng, L., 2017.
37 715 Prediction of diagenetic facies using well logs – a case study from the Upper Triassic
38 716 Yanchang Formation, Ordos Basin, China. *Marine and Petroleum Geology*, 81, 50-65.
- 39 717
- 40 718 55. Dickson, J.A.D., 1965. A modified staining technique for carbonates thin section.
41 719 *Nature*, 205, 587-588.
- 42 720
- 43 721 56. Al-Juboury, A., Howard, J.P., Vincent, S.J., Nichols, G., 2021. Petrography,
44 722 diagenesis and geochemistry of the Cambro-Ordovician Khabour sandstones, western
45 723 Iraq: Implications for reservoir quality and impact of the Hirnantian glaciation.
46 724 *Marine and Petroleum Geology*, 123, 104733.
- 47 725

726 57. Folk, R.L., 1980. Petrology of sedimentary rocks. Hemphill Publishing Company,
1 727 Austin, Texas.
2 728

3
4 729 58. Dutton, S.P., Hutton, M.E., Ambrose, W.A., Childers, A.T., Loucks, R.G., 2018.
5 730 Preservation of reservoir quality by chlorite coats in deep Tuscaloosa Sandstones,
6 731 Central Louisiana, USA. Gulf Coast Association of Geological Societies, 7, 46-58.
7 732

8
9 733 59. Bello, A.M., Al-Ramadan, K., Babalola, L.O., Alqubalee, A., Amao, A.O., 2023.
10 734 Impact of grain-coating illite in preventing quartz cementation: Example from permo-
11 735 carboniferous sandstone, Central Saudi Arabia. Marine and Petroleum Geology, 149,
12 736 106073.
13 737

14
15 738 60. Bello, A.M., Jones, S., Gluyas, J., Acikalin, S., Cartigny, M., 2021. Role played by
16 739 clay content in controlling reservoir quality of submarine fan system, Forties
17 740 Sandstone Member, Central Graben, North Sea. Marine and Petroleum Geology, 128,
18 741 105058.
19 742
20 743
21 744
22
23
24
25
26
27
28
29
30
31
32
33
34
35
36
37
38
39
40
41
42
43
44
45
46
47
48
49
50
51
52
53
54
55
56
57
58
59
60
61
62
63
64
65

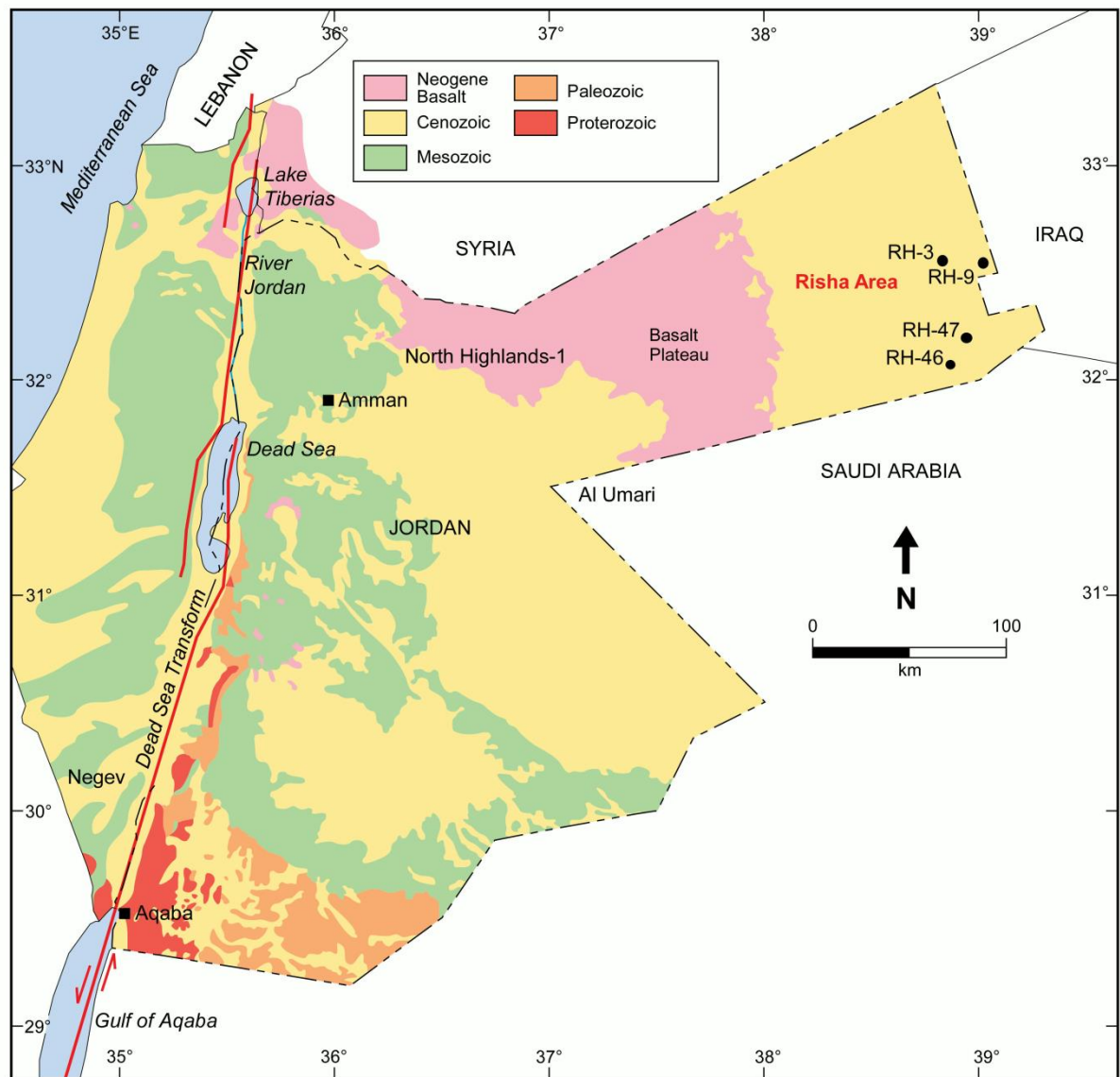


Fig. 1 Location map of the Risha gas field, north-eastern Jordan, along with the four well locations that have maximum data coverage, modified after Naylor et al. (2013)

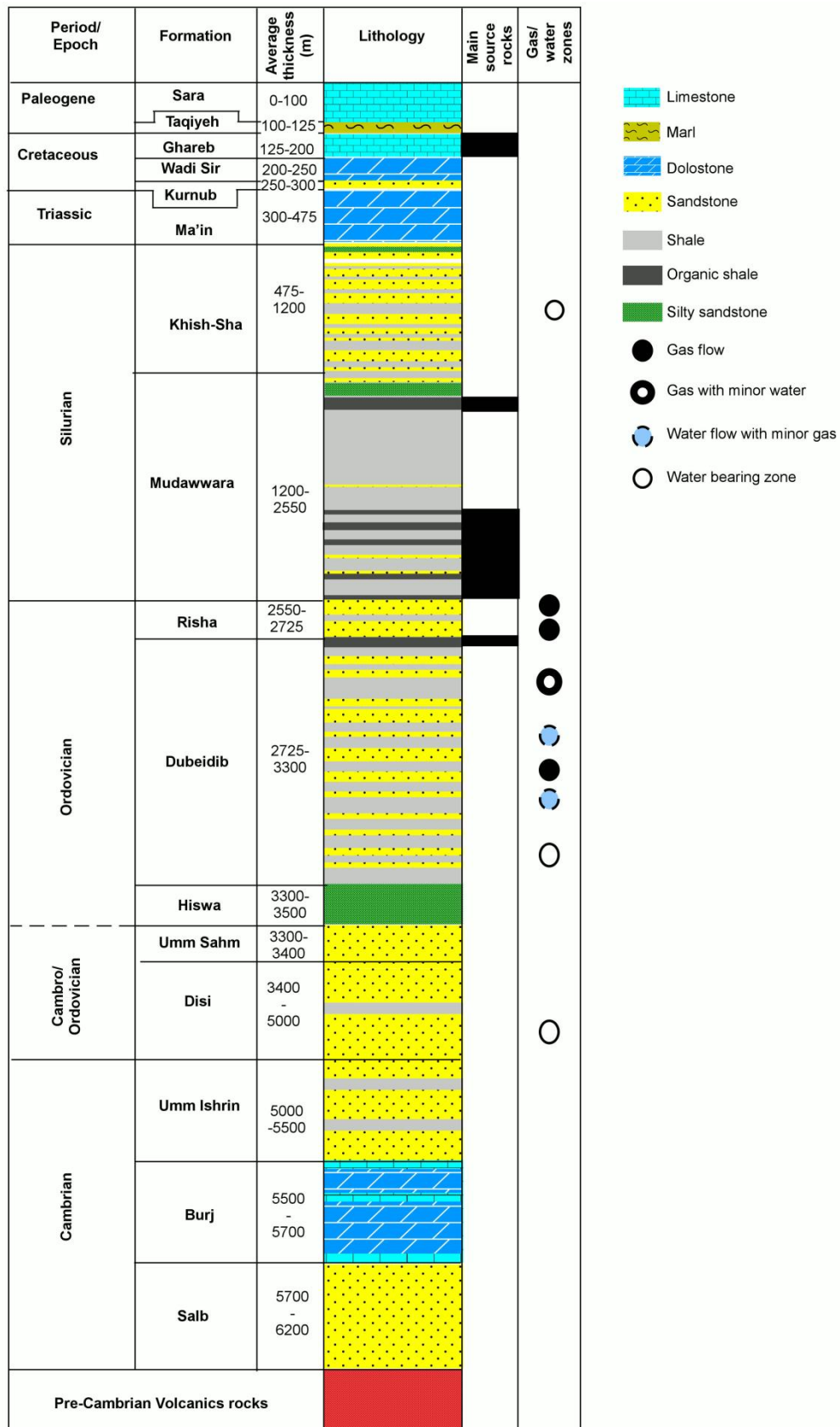


Fig. 2 Stratigraphic succession of the studied Risha gas field (Hakimi et al., 2023)

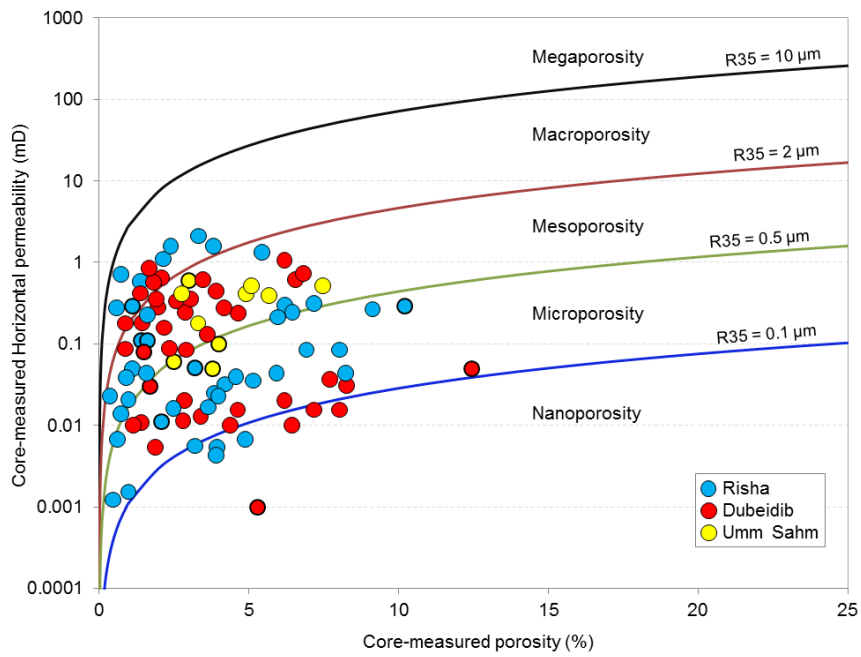


Fig. 3 Core-based porosity and permeability indicating the dominance of micro- and mesopores within the three studied formations from the Risha field

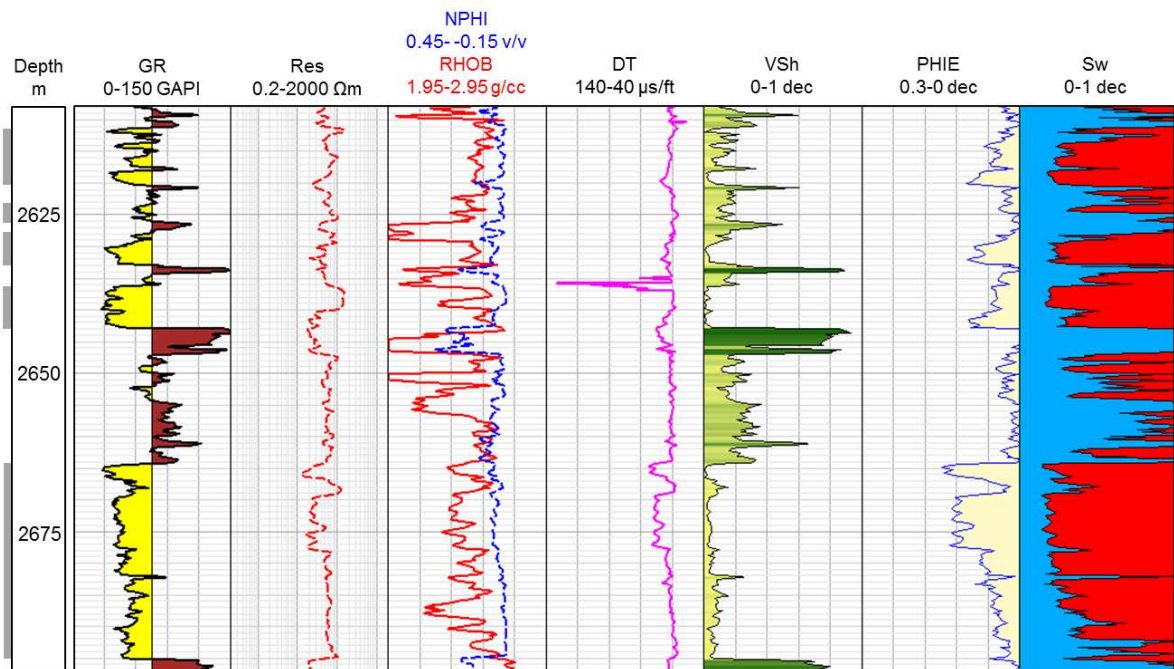


Fig. 4 Wireline logs and inferred key petrophysical properties of the Risha Formation in the well RH-3. Reservoir pay zones are marked in grey

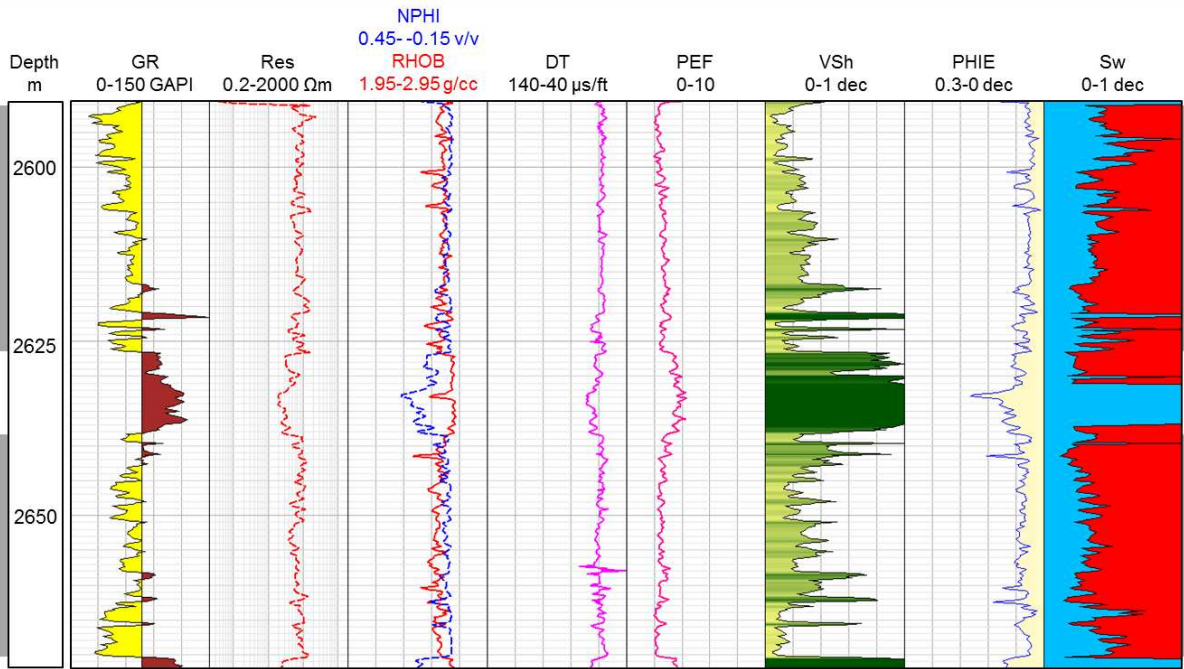


Fig. 5 Wireline logs and inferred key petrophysical properties of the Risha Formation in the well RH-9. Reservoir pay zones are marked in grey

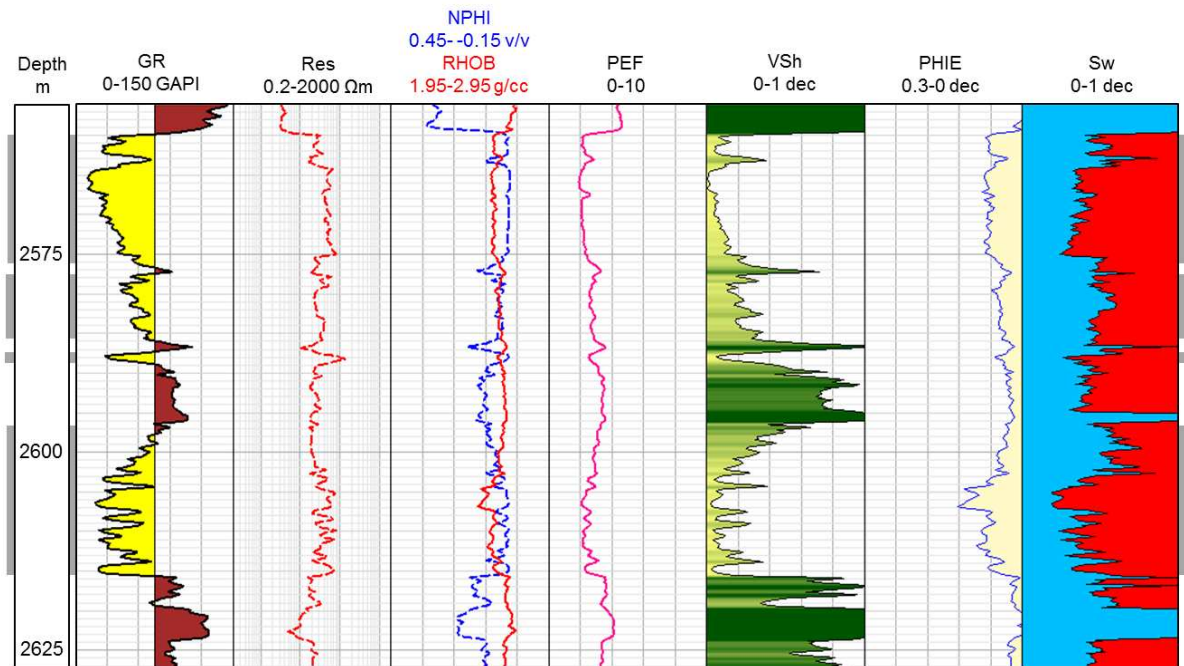


Fig. 6 Wireline logs and inferred key petrophysical properties of the Risha Formation in the well RH-46. Reservoir pay zones are marked in grey

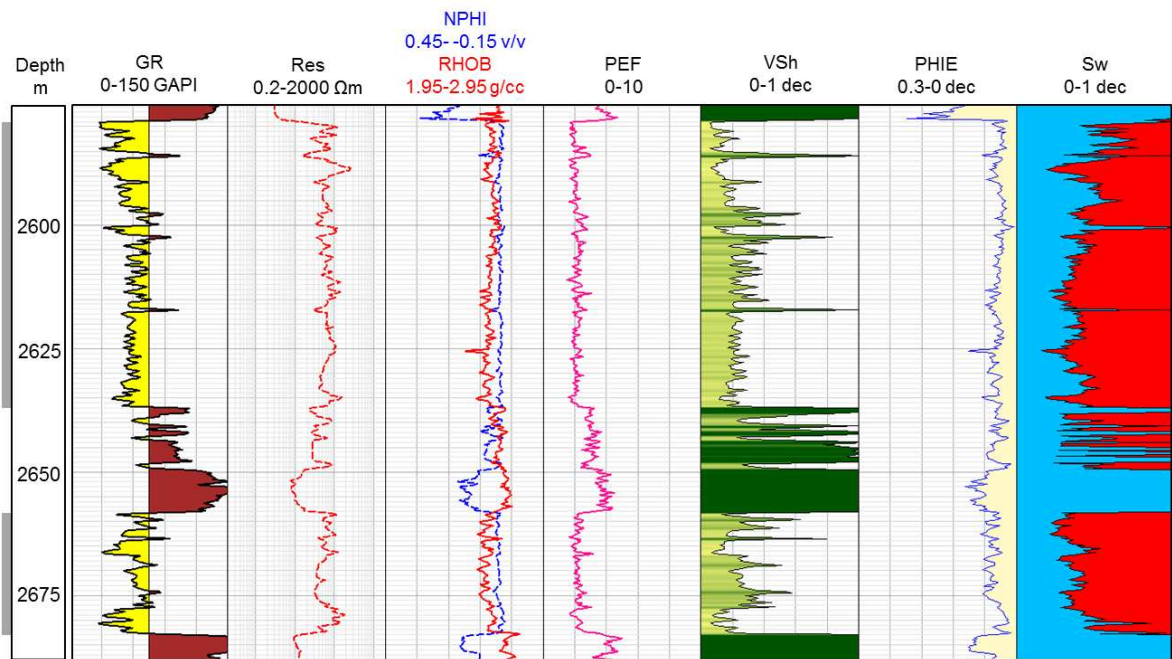


Fig. 7 Wireline logs and inferred key petrophysical properties of the Risha Formation in the well RH-47. Reservoir pay zones are marked in grey

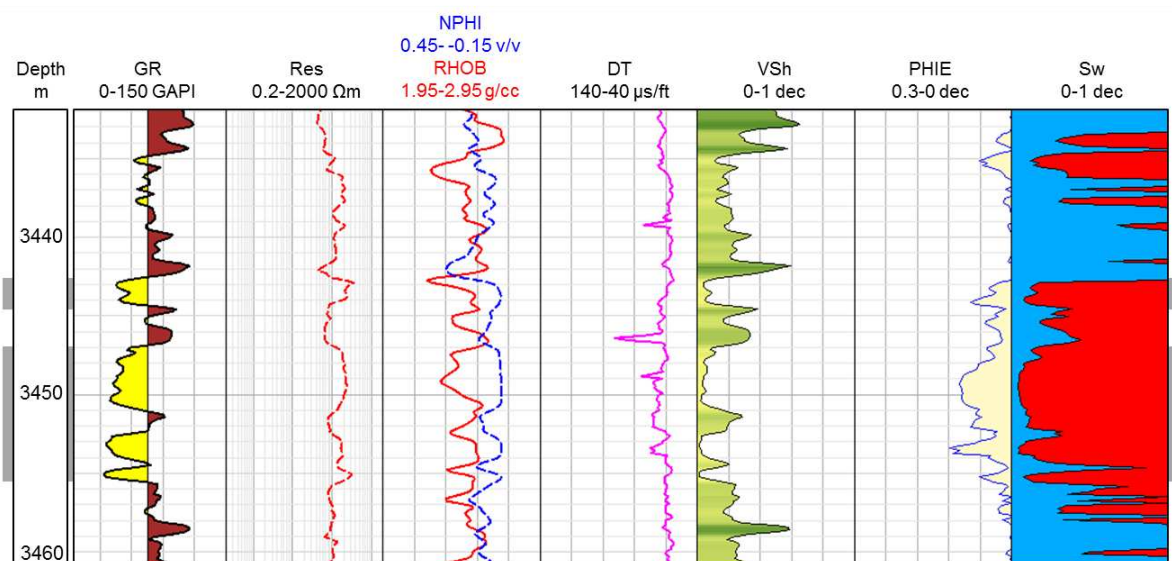


Fig. 8 Wireline logs and inferred key petrophysical properties of the Dubeidib Formation in the well RH-3. Reservoir pay zones are marked in grey

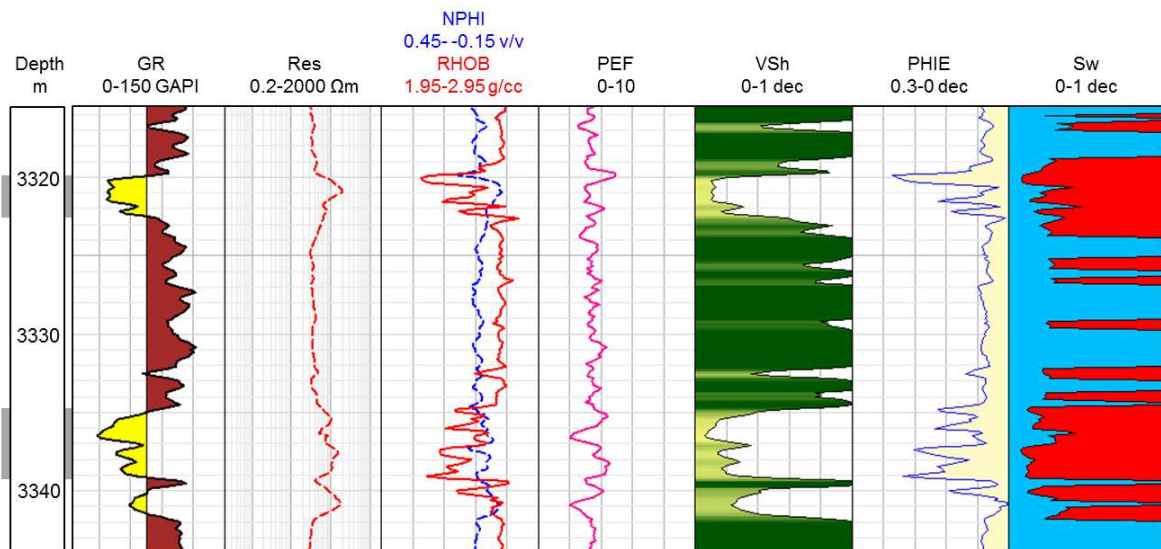


Fig. 9 Wireline logs and inferred key petrophysical properties of the Dubeidib Formation in the well RH-47. Reservoir pay zones are marked in grey

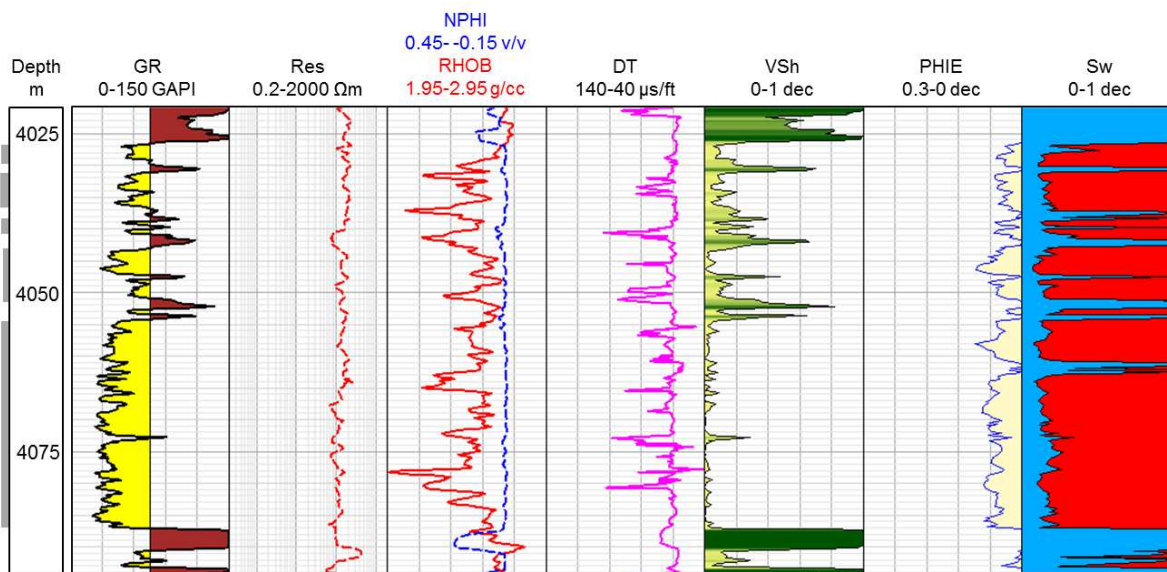


Fig. 10 Wireline logs and inferred key petrophysical properties of the upper Umm Sahn Formation in the well RH-3. Reservoir pay zones are marked in grey

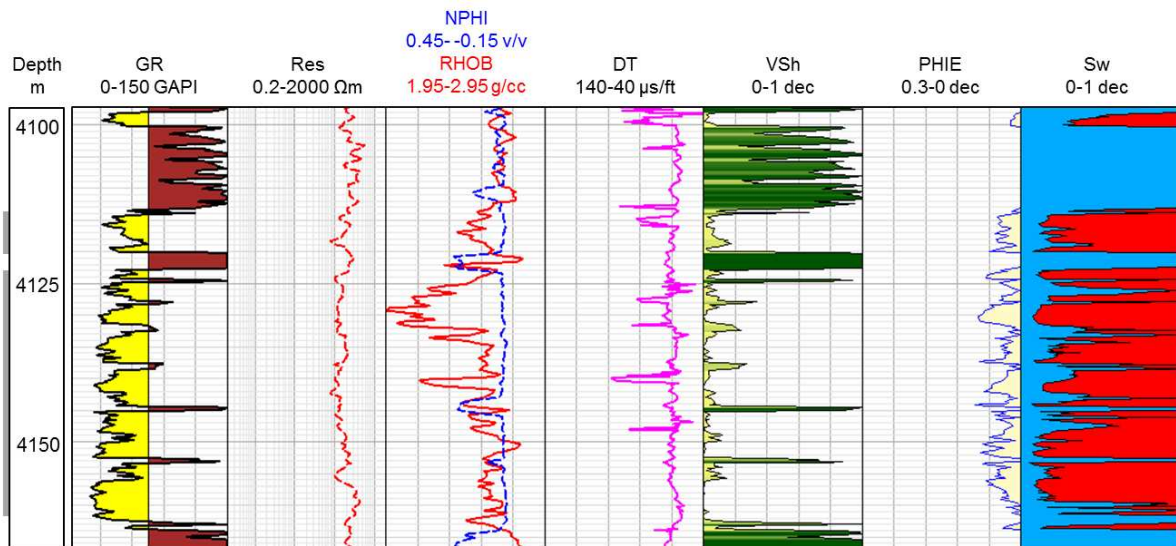


Fig. 11 Wireline logs and inferred key petrophysical properties of the lower Umm Sahn Formation in the well RH-3. Reservoir pay zones are marked in grey

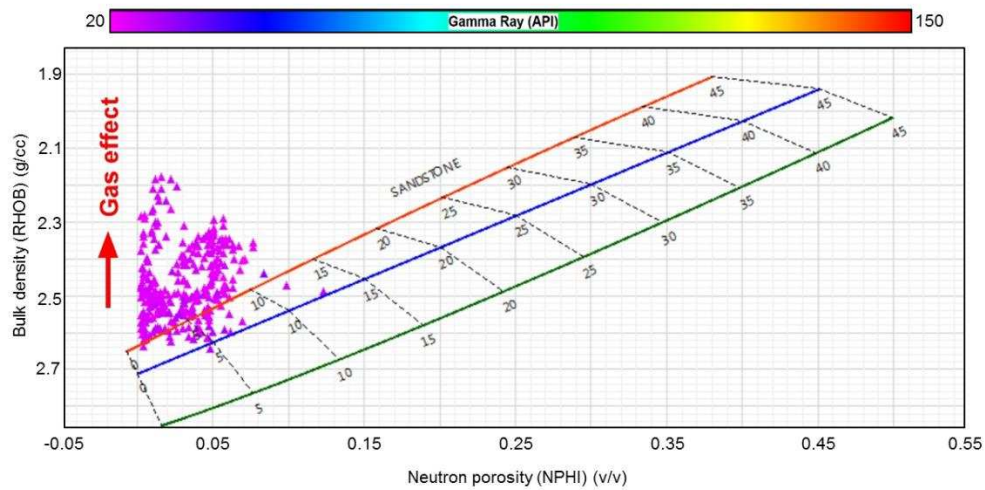


Fig. 12 Cross-plot between neutron porosity and bulk density indicating lithological compositions and gas effects in the Risha Formation pay zones from the well RH-3

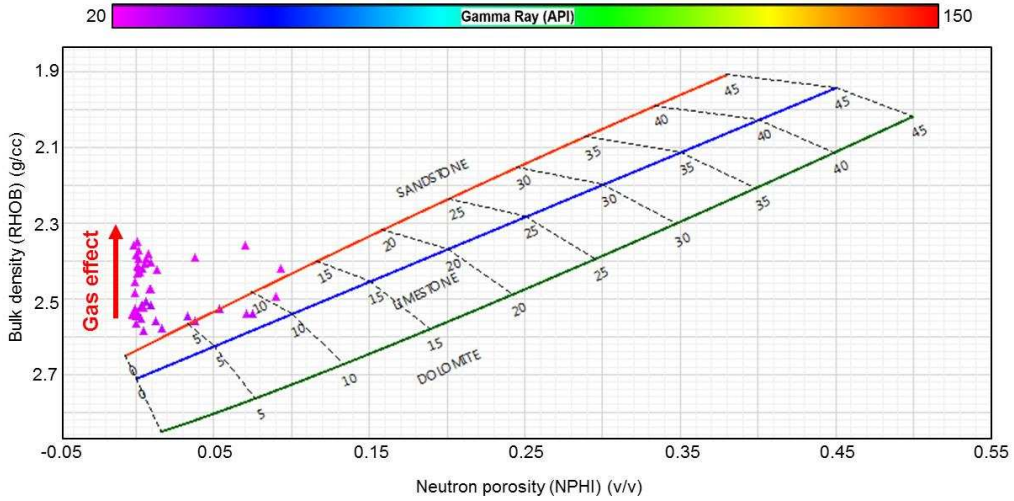


Fig. 13 Cross-plot between neutron porosity and bulk density indicating lithological compositions and gas effects in the Dubeidib Formation pay zones from the well RH-3

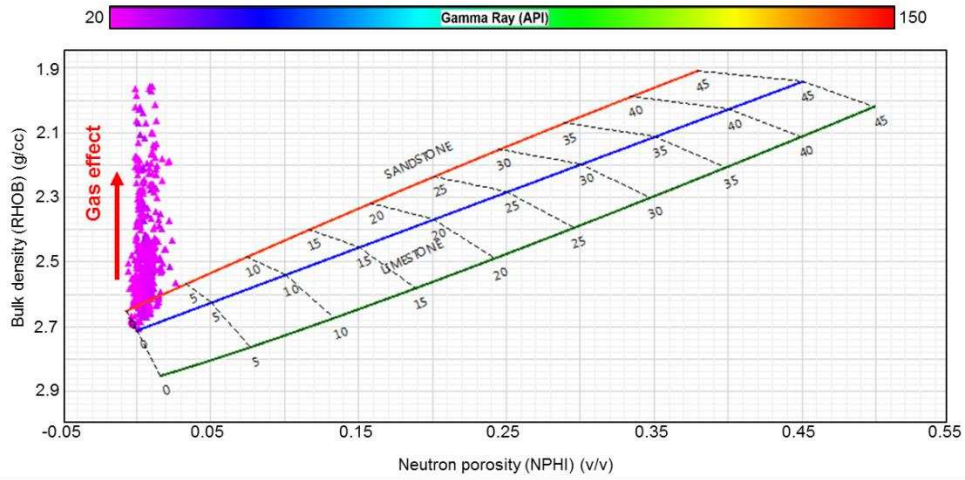


Fig. 14 Cross-plot between neutron porosity and bulk density indicating lithological compositions and gas effects in the Umm Sahm Formation pay zones from the well RH-3

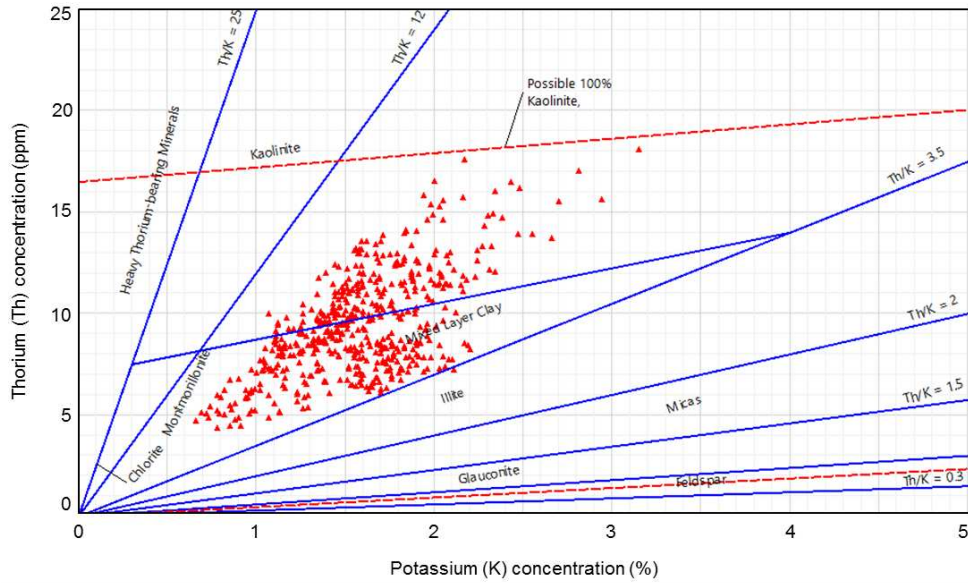


Fig. 15 Cross-plot between potassium (K) and thorium (Th) concentrations indicating montmorillonite, kaolinite, and mixed-layer clay as the dominant clay phases within the Risha Formation pay zones from the well RH-47

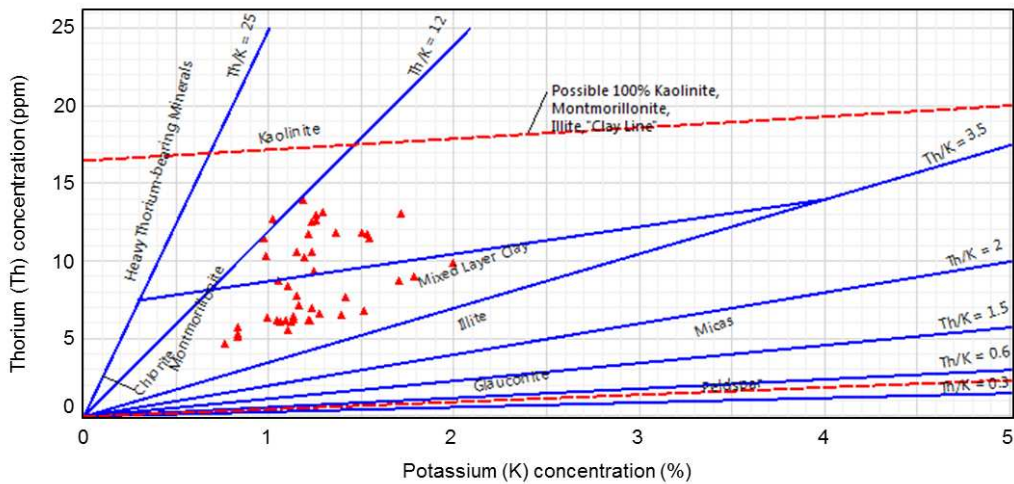


Fig. 16 Cross-plot between potassium (K) and thorium (Th) concentrations indicating montmorillonite, kaolinite, and mixed-layer clay as the dominant clay phases within the Dubeidib Formation pay zones from the well RH-47

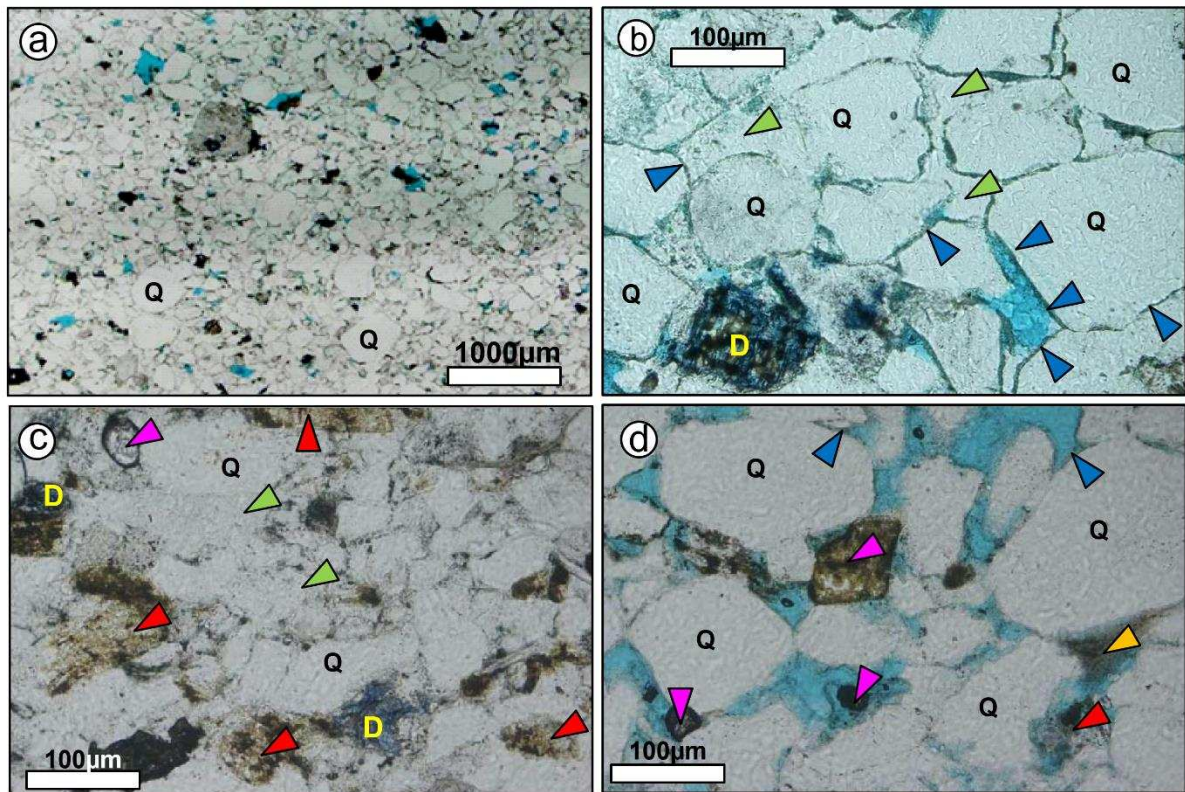


Fig. 17 Optical photomicrographs of the Risha Formation (reservoir pay zones) from (a-b) depth 2635.95m, well Risha-23, (c) depth 2660.25m, well Risha-25 and (d) depth 2677.53m, well Risha-25, indicating the dominant quartz grains (Q), subordinate amount of fresh to partially altered/dissolved feldspar (red arrow), pore-filling detrital clay (orange arrow), chlorite rims surrounding quartz framework grains (blue arrow), minor ferroan dolomite (D) and extensive pore-filling quartz cement (green arrow), along with trace amounts of heavy minerals (pink arrow). Primary interparticle macropores are present (impregnated with blue-dyed resin)

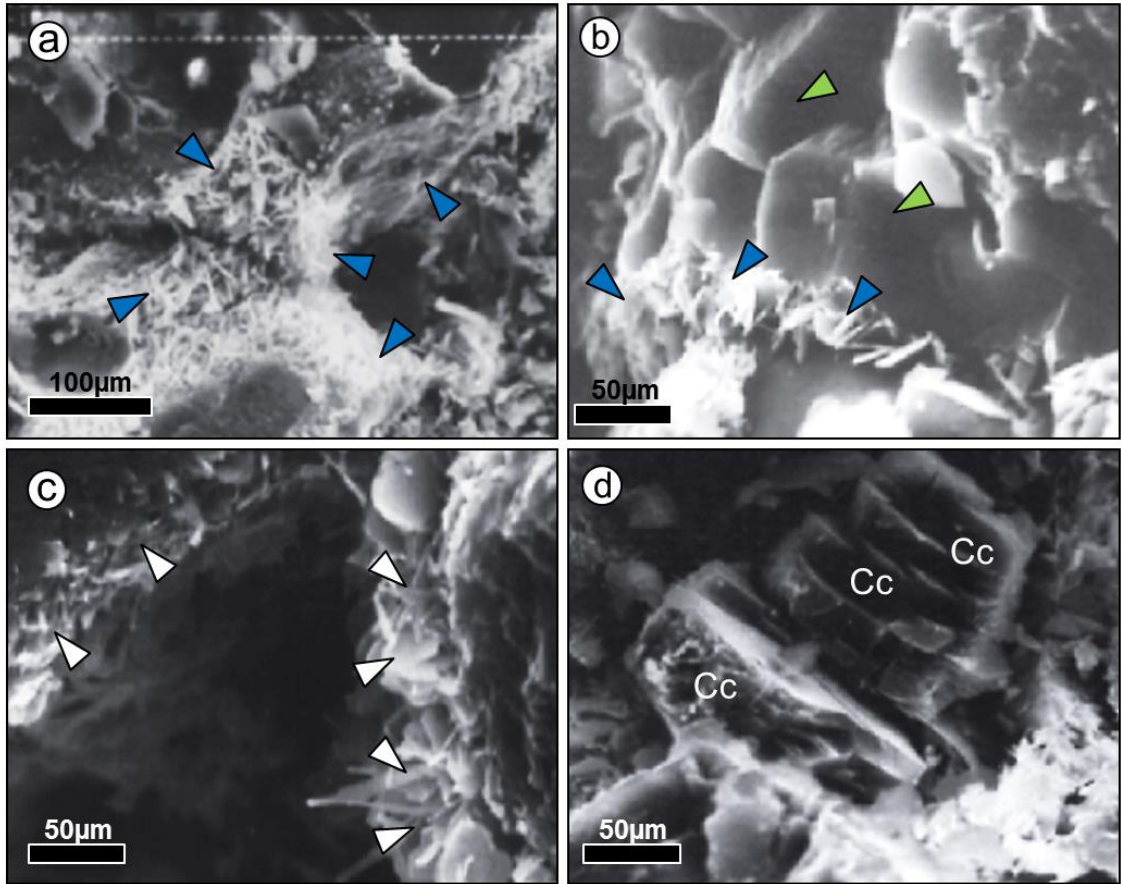


Fig. 18 (a-d) Scanning electron microscope (SEM) images of the Risha sandstones from the well RH-29 at a depth of 2684.7m indicating pore-filling, grain-coating, and pore-lining chlorites (blue arrow), quartz cementation (green arrow), pore-lining illite (white arrow) and carbonate cement (Cc)

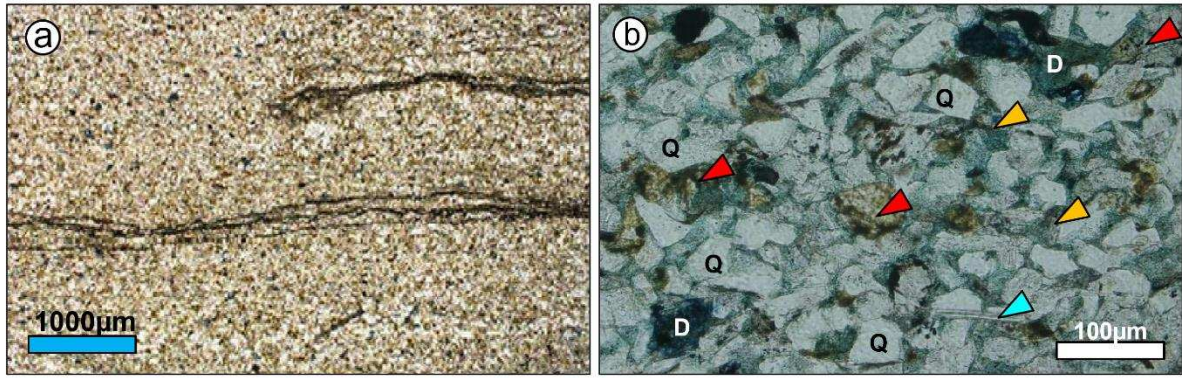


Fig. 19 Optical photomicrographs of the Dubeidib Formation (reservoir pay zones) from (a) depth 3335.03m, well RH-47 exhibiting very fine-grained sandstone-siltstone with laminated clay fabric and starry night appearance, (b) depth 2939.55m, well Risha-23, indicating abundant quartz grains (Q), subordinate amount of fresh to partially altered/dissolved feldspar (red arrows), pore-filling detrital clay (orange arrows) and minor ferroan dolomite (D) along with trace amounts of mica (aqua blue arrow)

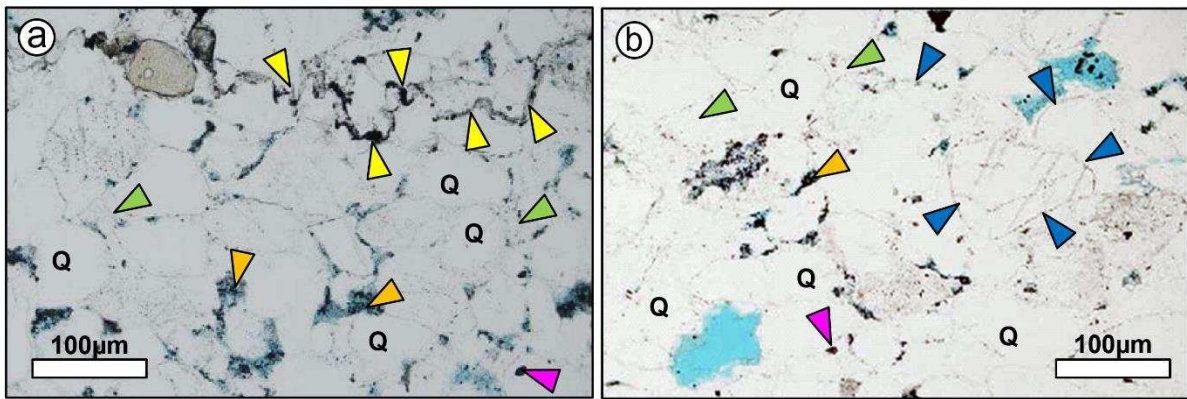


Fig. 20 Optical photomicrographs of the Umm Sahn Formation (reservoir pay zones) from (a) depth 4292.7m, and (b) depth 4191.5m, well RH-47, indicating abundant quartz (Q) framework grains, chlorite rims surrounding quartz grains (blue arrows), pore-filling clay (orange arrows), locally sutured grain contacts and stylolites (yellow arrows) and extensive pore-filling quartz cement (green arrows), along with minor amounts of heavy minerals (pink arrow). Pore spaces are impregnated with blue-dyed resin

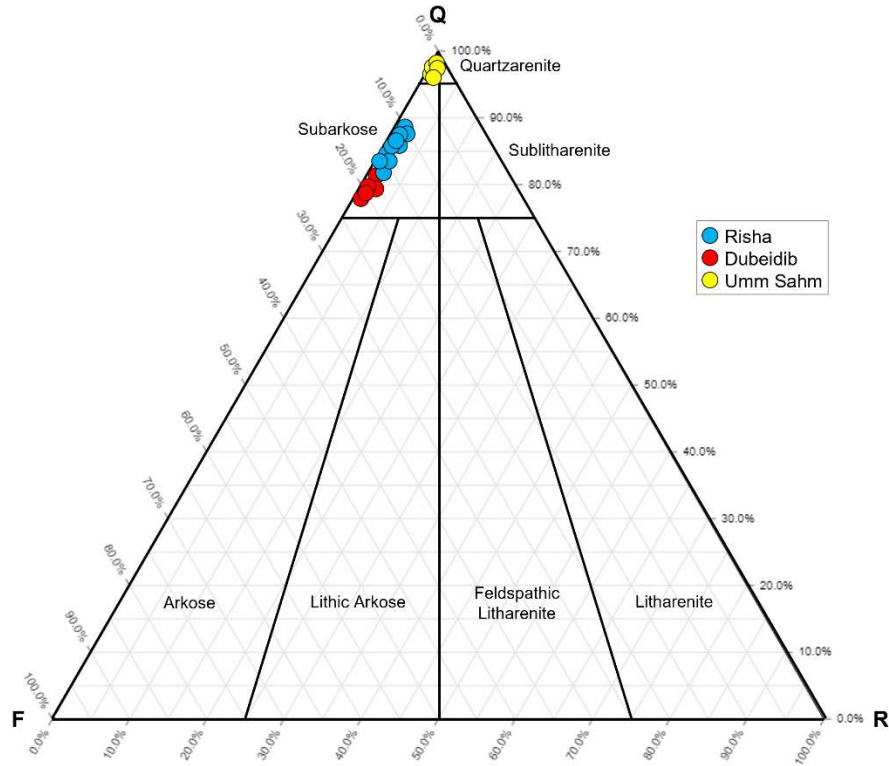


Fig. 21 QFR diagram showing the composition of the three studied sandstone reservoir intervals, constructed after Folk [57]. The plot shows that the Risha and Dubeidib sandstones are subarkose and the Umm Sahn sandstones are Quartzarenite.

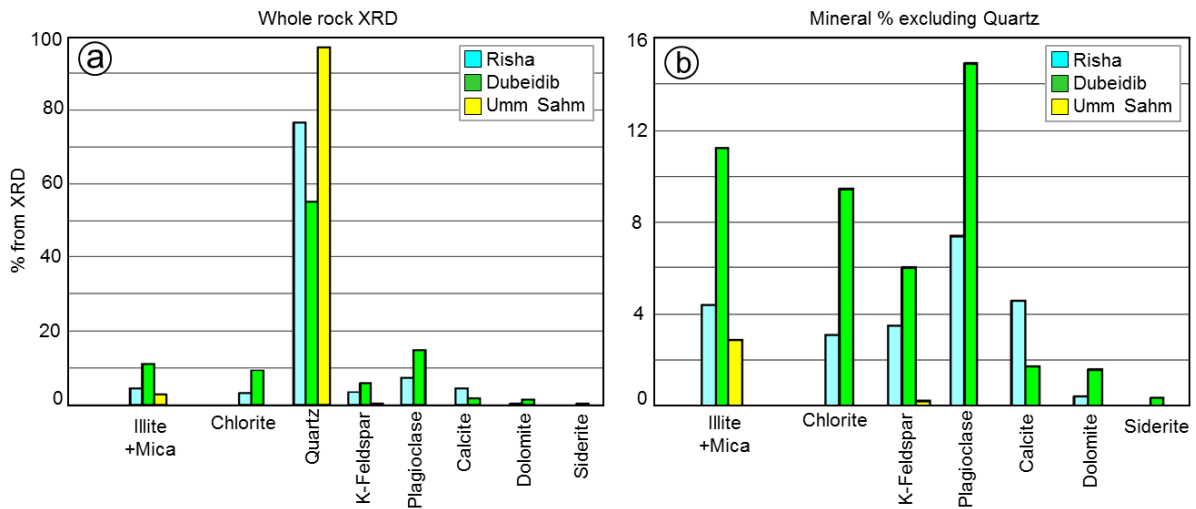


Fig. 22 (a) Whole-rock X-ray diffraction (XRD) results, and (b) mineral distributions excluding quartz from the Risha Formation (23 samples), Dubeidib Formation (7 samples), and Umm Sahn Formation (3 samples) in the Risha Field

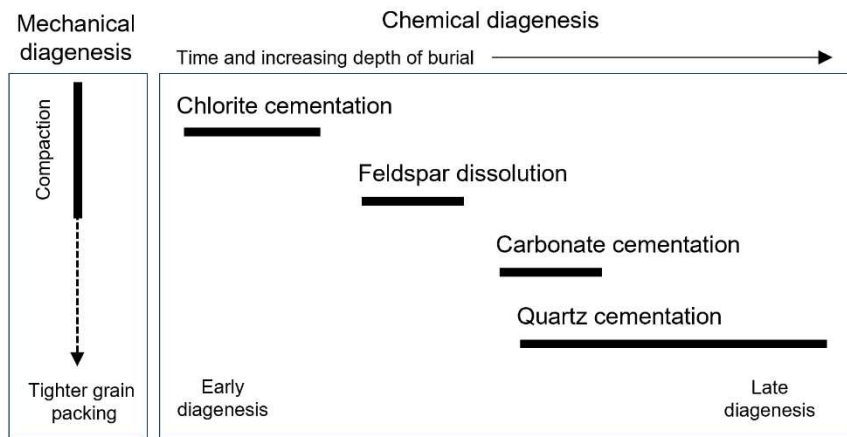


Fig. 23 The paragenetic sequence of the main diagenetic features observed in the studied sandstones.

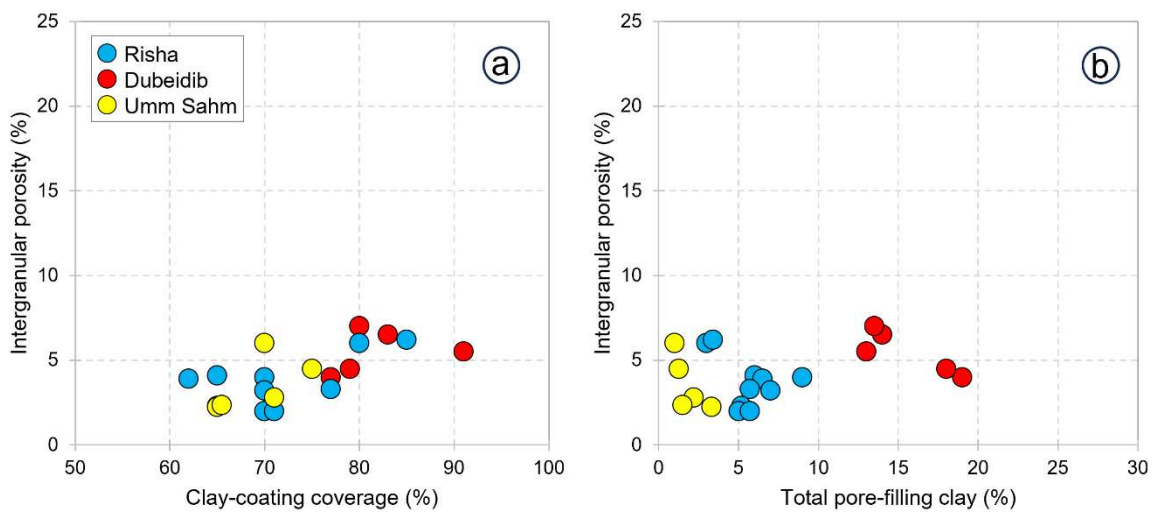


Fig. 24 Impact of clay-coating coverage and pore-filling clays on intergranular porosity. (a) plot of intergranular porosity against clay-coating coverage indicating a minor increase in intergranular porosity with increasing clay-coating coverage on detrital grains, (b) plot of intergranular porosity against total pore-filling clay indicating higher clay content in the Dubeidib sandstones.

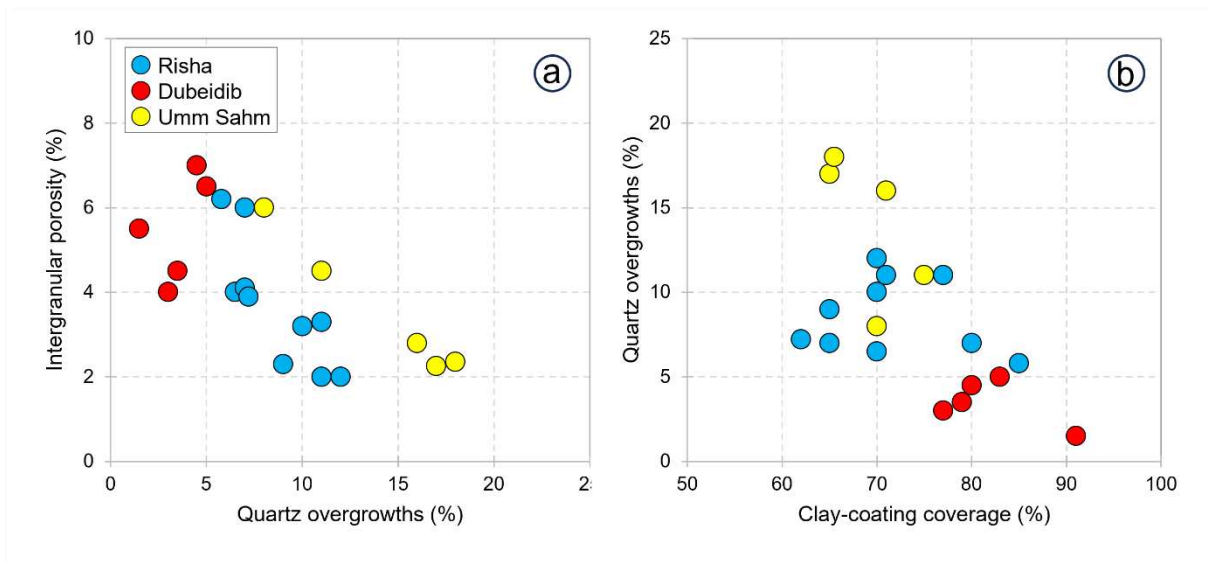


Fig. 25 Relation between quartz overgrowths with intergranular porosity and clay-coating coverage. (a) plot of intergranular porosity against quartz overgrowth indicating a decrease in intergranular porosity with increasing quartz cement volume, (b) plot of quartz overgrowth against clay-coating coverage indicating a decrease in quartz cement volume with increasing clay-coating coverage.

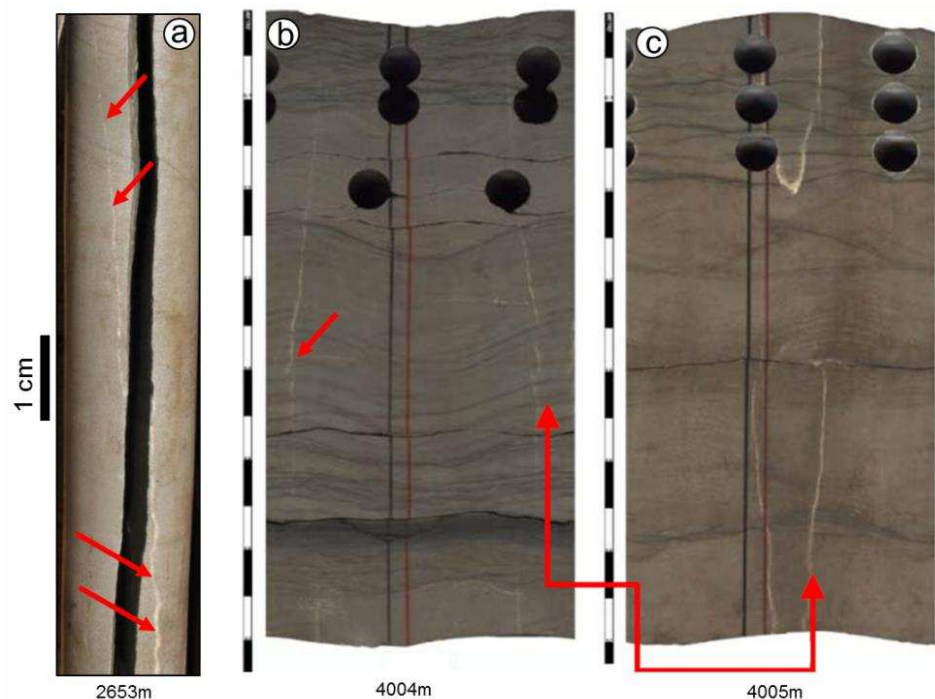


Fig. 26 Core photographs of calcite-filled thin natural fractures (marked by red arrows) within the studied (a) Risha Formation, well RH-25, depth 2653m and (b) Umm Sahn Formation, well RH-47, depth 4004-4005m from the Risha Field

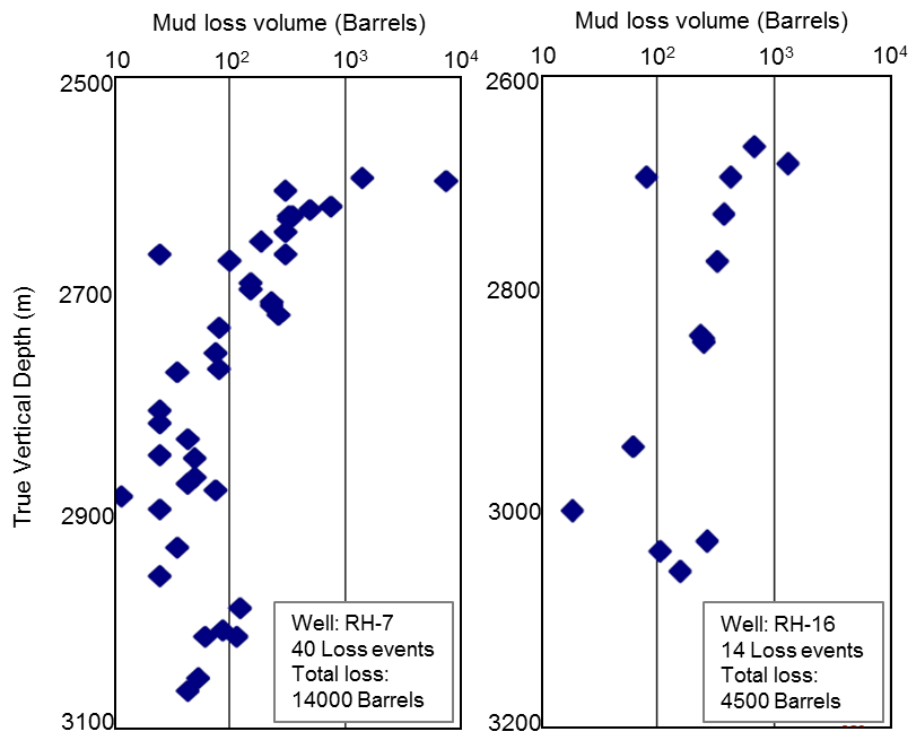


Fig. 27 Mud loss events encountered during drilling through the Risha Formation from the wells RH-7 and RH-16

Table 1. Summary table for the estimated key petrophysical properties of the promising reservoir intervals from the three studied formations. Vsh= shale volume, PHIE= effective porosity, Sw= water saturation and Sh= hydrocarbon saturation.

Formation	Well name	Reservoir Interval (m)		Thickness (m)	Vsh dec	PHIE dec	Sw dec	Sh dec	Figure No.
		From	To						
Risha	RH-3	2610	2695	85	3-10	6-15	15-35	65-85	4
	RH-9	2590	2670	80	5-30	6-10	25-40	60-75	5
	RH-46	2560	2615	55	5-20	6-12	20-55	45-80	6
	RH-47	2580	2680	100	5-20	5-10	35-55	45-65	7
Dubeidib	RH-3	3442	3456	14	2-5	5-10	5-10	90-95	8
	RH-47	3320	3341	21	10-20	6-12	10-20	80-90	9
Umm Sahm	RH-47 Upper zone	4025	4085	60	2-5	5-7	10-20	80-90	10
	RH-47 Lower zone	4115	4160	45	0-5	4-6	15-25	75-85	11